1 **Role of atmospheric aerosols in severe winter fog over Indo Gangetic Plains of India: a**
2 **case study**

3 Chandrakala Bharali[1], Mary Barth[2], Rajesh Kumar[2], Sachin D. Ghude[3], Vinayak Sinha[4], Baerbel Sinha[4]

4 [1] Dibrugarh University, Dibrugarh, Assam, India

5 [2] NSF National Centre for Atmospheric Research, Boulder, CO, US

6 [3] Indian Institute of Tropical Meteorology, Ministry of Earth Sciences, Pune, India

7 [4] Department of Earth and Environmental Sciences, Indian Institute of Science Education and Research, Mohali,
8 Punjab, India

9 **Correspondence:** chandrakalabharali@gmail.com, barthm@ucar.edu

11 **Abstract**

12 Winter fog and severe aerosol loading in the boundary layer over north India, especially in the Indo-
13 Gangetic Plain (IGP), disrupts the daily lives of millions of people in the region. To understand better
14 the role of aerosol-radiation feedback on the occurrence, spatial extent, and persistence of winter fog;
15 and the associated aqueous chemistry in fog in the IGP, several model simulations have been
16 performed using the Weather Research and Forecasting model coupled with chemistry (WRF-Chem).
17 While WRF-Chem was able to represent the fog formation for the December 23-24, 2017 fog event
18 over the central IGP in comparison to station and satellite observations, the model underestimated
19 $PM_{2.5}$ concentrations compared to the Central Pollution Control Board of India monitoring network.
20 While evaluating aerosol composition for fog events in IGP, we found that the WRF-Chem aerosol
21 composition was quite different from measurements obtained during the Winter Fog Experiment in
22 Delhi, with secondary aerosols, particularly chloride aerosol fraction being strongly underpredicted
23 (~66.6%). Missing emission sources (e.g., industry and residential burning of cow dung and trash) and
24 aerosol and chemistry processes need to be investigated to improve model-observation agreement. By
25 investigating a fog event on December 23-24, 2017 over central IGP, we found that the aerosol-
26 radiation feedback weakens turbulence, lowers the boundary layer height, and increases $PM_{2.5}$
27 concentrations and RH within the boundary layer. Factors affecting the feedback include loss of
28 aerosols through deposition of cloud droplets and internal mixing of absorbing and scattering aerosols.
29 Aqueous-phase chemistry increases the $PM_{2.5}$ concentrations, which subsequently affects the aerosol-
30 radiation feedback by both increased mass concentrations and aerosol sizes. With aerosol-radiation
31 interaction and aqueous phase chemistry, fog formation began 1-2 hours earlier and caused a longer
32 fog duration than when these processes were not included in the WRF-Chem simulation. The increase
33 in RH in both the experiments is found to be important for fog formation as it promoted the growth of
34 aerosol size through water uptake, increasing the fog water content over IGP. The results from this

study suggest that the aerosol-radiation feedback and secondary aerosol formation play an important role in the air quality and the intensity and lifetime of fog over IGP, yet other feedbacks, such as aerosol-cloud interactions, need to be quantified.

1   Introduction

The Indo-Gangetic Plain (IGP; 21°35′-32°28′N latitude. and 73°50′-89°49′E longitude) in the northern part of the Indian subcontinent is one of the most densely populated and heavily polluted regions in South Asia. The rapid population and economic growth in the IGP region over the last decade have increased air pollution over this region. This is evident from the increasing trend in AOD and NO_2 column concentration over India reported in recent studies (Dey and Di Girolamo, 2011; Ghude et al., 2013; Krishna Moorthy et al., 2013), which has slowed and reversed only recently (Sarkar et al., 2019). The high concentration of aerosols along the IGP and their adverse effects on human health and the environment are increasing (Ghude et al., 2016). Consequently, more than 500 million people living in the IGP breathe air that exceeds the National Ambient Air Quality Standards (NAAQS), which has reduced the life expectancy of the people (Debnath et al., 2022; Lelieveld et al., 2015). Lelieveld et al., (2015) estimated a very high number of premature deaths (0.716 million per year) linked to aerosols ($PM_{2.5}$), thus making Southeast Asia one of the largest regions affected by premature mortality globally.

One of the major environmental concerns in the IGP is the urban air quality during winter, especially over the mega-cities, e.g., Delhi, located in the north-western part of IGP (Ghude et al., 2020; Jena et al., 2021; Sengupta et al., 2022). Several urban air pollution hotspots along the IGP extend from northwest to east with monthly average $PM_{2.5}$ greater than 200 μgm^{-3} (NAAQS=60μgm^{-3}, 24 hr average) in the winter season (Bharali et al., 2019; Krishna et al., 2019). IGP is dominated mainly by fine mode particulates, especially over central to eastern IGP, during post-monsoon and winter (Kumar et al., 2018). Biomass burning (agricultural waste burning, domestic heating, etc.) is an important contributor to the observed high $PM_{2.5}$ loading over IGP during these seasons (Kulkarni et al., 2020; Pant et al., 2015; Pawar and Sinha, 2022; Sharma et al., 2010; Yadav et al., 2020). Delhi is affected substantially by the emissions from agricultural waste burning in the north-western states of Punjab and Haryana during the post-monsoon (October-November) season (Badarinath et al., 2009; Jethva et al., 2018; Kumar et al., 2021). Studies showed that $PM_{2.5}$ increased from ~50 $\mu g\ m^{-3}$ to as high as 300 $\mu g\ m^{-3}$ (Ojha et al., 2020), and AOD reached 0.98 with the presence of absorbing aerosols (Singh et al., 2018) during the peak biomass burning in post-monsoon.

IGP experiences fog (both radiation and advection fog) every winter after the passage of the synoptic wind system called the "Western Disturbances". The majority of fog events in the IGP during December-January are radiation fog (Deshpande et al., 2023; Ghude et al., 2023), formed due to radiative cooling of the surface. The number of low visibility days due to haze/fog formation has been

71 increasing significantly (Ghude et al., 2017; Jenamani, 2007; Singh and Dey, 2012), impacting socio-
72 economic activities, e.g., aviation (Kulkarni et al., 2019). The increase in the intensity and regional
73 extent of fog over IGP is consistent with the increasing trend in aerosol concentration due to
74 increasing anthropogenic emissions (Sarkar et al., 2006; Syed et al., 2012).

75   Several factors control the formation and persistence of fog in the IGP, e.g., stable boundary
76 layer, low temperature, availability of moisture (supplied by the Western Disturbances and irrigation
77 activities), and the aerosol number and composition (Acharja et al., 2022; Dhangar et al., 2021). It has
78 also been suggested that the atmospheric rivers (moisture incursion from Arabian Sea) act as a source
79 of water vapor over IGP, which fuels the intensification of fog and haze (Verma et al., 2022) during
80 winter. The high aerosol concentration in the boundary layer influences fog formation (Gautam et al.,
81 2007; Safai et al., 2019) over the IGP by providing the needed cloud condensation nuclei (CCN) for
82 activation into fog droplets. In addition, aerosols induce surface cooling by reducing solar radiation at
83 the surface while warming the lower troposphere by absorption (Ding et al., 2016; Yu et al., 2002). A
84 reduction in surface-reaching solar radiation by ~19% has been reported during winter over Kanpur in
85 the IGP (Dey and Tripathi, 2007). The reduced solar flux affects the boundary layer stability and
86 depth by suppressing the thermals and thus further increasing the surface aerosol concentration via
87 aerosol-radiation feedback, which is very strong over the IGP (Bharali et al., 2019). Kumar et al.,
88 (2020) have shown that aerosol-radiation feedback significantly improves the accuracy of $PM_{2.5}$ and
89 temperature forecasts in Delhi. Srivastava et al., (2018) reported that the direct aerosol forcing over
90 polluted regions is very large with values up to -80.0 ± 7.2 W m^{-2} over the IGP in the winter season.

91   Aerosol-radiation interaction determines that the aerosol distribution is critical for the evolution
92 of fog (Bodaballa et al., 2022; Steeneveld et al., 2015), while microphysics is important for fog
93 formation and dispersal (Boutle et al., 2018; Maalick et al., 2016). Although the relationship between
94 the aerosol chemical composition and aerosol activation to CCN has not been fully understood yet,
95 studies have found that the chemical composition and mixing state of aerosols affect the
96 hygroscopicity (κ) of aerosols (Bodaballa et al., 2022; Ma et al., 2013; Moore et al., 2012; Zhang et
97 al., 2014a). Fog processes involve a complex interplay between local meteorology, radiation,
98 microphysics, and aerosol chemistry, making it difficult to understand the fog lifecycle (Acharja et al.,
99 2022; Maalick et al., 2016; Zhang et al., 2014b). There is considerable heterogeneity in the spatial and
100 temporal aerosol properties over IGP and the poor estimates of their mixing state. Therefore,
101 prediction of fog by weather models is still challenging with biases in fog's onset and dispersal
102 timings.

103   Previous studies have focussed on the impacts of meteorological conditions, topography, or
104 anthropogenic emissions on the poor air quality and intensification of fog during winter over IGP (e.g.
105 Hakkim et al., 2019). However, studies on the effect of feedback induced by the aerosols on the
106 meteorological conditions and thus on aerosol concentration are very limited over this region, except
107 for a few above-mentioned studies which discuss how the aerosol-radiation feedback favors haze and

108 fog during winter. Moreover, fog can provide a medium for aqueous-phase reactions. While several
109 earlier studies have reported an increase in secondary aerosols during fog over IGP, a sensitivity study
110 examining the impact of fog on aqueous phase chemistry has not yet been done over IGP.

111   In the present work, we aim to find the suitable chemistry/physics as well as the meteorology
112 initial/boundary conditions that lead to improved simulations of fog events in the Weather Research
113 and Forecasting model coupled with chemistry (WRF-Chem; (Fast et al., 2006; Grell et al., 2005;
114 Powers et al., 2017). We also explore the role of aerosol-radiation feedback on fog properties as the
115 high aerosol loadings in northern India can impact the heating rates, temperature inversions, and
116 boundary layer height. The role of aqueous chemistry on fog properties and vice-versa is also
117 investigated.

118

119   2   Methodology

120 Fog formed due to radiative cooling at the surface on both 23rd and 24th December 2017 over a
121 widespread region of the IGP (Fig. 1a, b). The fog region is located over an area with high $PM_{2.5}$
122 anthropogenic emissions (Fig. 1c). The IGP is a large region with varying meteorology and aerosol
123 characteristics, therefore, it is divided into three areas, northwest (NWIGP: latitude-longitude range,
124 27°N-32°N,75°E-79°N), central (CIGP: latitude-longitude range, 25°N-28°N,79°E-83°E), and east
125 (EIGP: latitude-longitude range, 24°N-27°N, 83°E-87°E) which are marked by the black rectangles in
126 Fig.1c. Although biomass burning and anthropogenic emissions dominate throughout the IGP during
127 post-monsoon and winter season, the north-westerly wind system results in the gradient distribution of
128 AOD over this region. The downwind regions, CIGP and EIGP are influenced by the long-range
129 transport from the NWIGP, resulting in high AOD with dominant fine particulates over CIGP and
130 EIGP, especially during post-monsoon and winter (Kedia et al., 2014; Kumar et al., 2018). Therefore,
131 representative stations from each region listed in section 2.2 are considered for the sensitivity
132 analyses.

133

134 2.1 Modeling

135   The WRF-Chem model version 4.0.3 is used for this study. Earlier studies have successfully
136 used WRF-Chem to predict fog (Pithani et al., 2019) and in the study of aerosol-radiation feedback on
137 air quality (Kumar et al., 2020; Bharali et al., 2019) and fog (Shao et al., 2023). The model domain is
138 centered at Delhi (77.1°E, 28.7°N) with 300 grid points in the east-west, 170 grid points in the south-
139 north direction (Fig. 1c), and 50 vertical eta levels with the model top at 50 hPa. The horizontal grid
140 spacing of the domain is 10 km, while the vertical grid spacing varies from higher resolution (~200 m)
141 in the boundary layer to coarser resolution (~1200 m) near the model top. We conduct three model
142 configurations (Table 1) for December 20-24, 2017 to identify the best configuration for
143 meteorological simulations. The three experiments have been designed with different combinations of
144 meteorological initial/lateral boundary conditions and planetary boundary layer (PBL) physics.

Experiment 1 (EXP1) uses the National Centers for Environmental Predictions (NCEP) Final Analysis (GFS-FNL; 1° x1°, 6 hourly) meteorology data for initial and boundary conditions and the YSU (Yonsei University; (Hong et al., 2006) PBL scheme. Experiments 2 and 3 (EXP2, EXP3) use ERA-Interim Project (1.125° x 0.703°, 6 hourly) for meteorology initial and boundary conditions. EXP2 uses the YSU PBL scheme while EXP3 uses the ACM2 (Asymmetric Convective Model version 2) PBL scheme. ACM2, is a hybrid of the original nonlocal closure (Pleim and Chang, 1992) and a local closure eddy diffusion scheme (Pleim, 2007a, 2007b). The YSU PBL option was coupled with the Noah LSM while ACM2 was coupled with Pleim-Xiu LSM. While YSU permits investigations of both aerosol-radiation (AR) and aerosol-cloud interactions, aerosol-cloud interactions are not possible when using the ACM2 PBL scheme because the ACM2 PBL scheme does not provide the exchange coefficient for heat, which is required to calculate the activation fraction for mass and number for each bin/mode. ACM2, on the other hand, has been shown to perform well for air quality in the IGP (Mohan and Gupta, 2018), however, they tested the YSU and ACM2 schemes during the summer time (1-15 June 2010) and focused on the evaluation of temperature, wind speed, PBL height, ozone, and PM_{10}. To ensure that model captures all the relevant meteorological parameters including relative humidity reasonably well during fog in winter, we designed EXP1, EXP2 and EXP3.

The advantage of Pleim-Xiu LSM (PX-LSM) is that it allows nudging of soil moisture and temperature to improve the prediction of meteorology near the surface (Pleim and Gilliam, 2009; Pleim and Xiu, 2003; Xiu and Pleim, 2001) which Noah LSM does not include. The PX-LSM includes two-layer soil (0–1 and 1–100 cm) model, canopy moisture, and aerodynamic and stomatal resistance. Ground surface (1 cm) temperature is calculated from the surface energy balance using a force-restore algorithm for heat exchange within the soil. Although the two-layer approach in PX-LSM is less detailed than the multilayer soil models such as the Noah LSM (four soil layers; Chen and Dudhia 2001), it performs well with realistic initialization for soil moisture and through dynamic adjustment in the model simulation where soil moisture is indirectly nudged according to differences in 2-m temperature (T2) and 2-m relative humidity (RH) between the model and observation (Pleim and Xiu, 2003).Soil moisture nudging adjusts the surface evaporation (direct soil surface evaporation, vegetative evapotranspiration, and evaporation from wet canopies) which then affects the partitioning of available surface energy into latent and sensible heat flux and thus reduces errors in T2 and 2-m RH.

For EXP2, meteorological initial conditions were refreshed every 24 hours, while EXP3 was a continuous run but soil moisture was nudged to the Era-Interim dataset to improve the prediction of surface fluxes. All other physics and chemistry options are the same for all the experiments except the surface physics option, which changes with the PBL scheme used. The deposition of cloud droplets is an important moisture and aerosol sink during fog events. For all these simulations, the deposition velocity of cloud droplets was reduced to 0.01 m s^{-1} based on Stoke's Law and previous studies (Katata et al., 2015; Tav et al., 2018) because its default value (0.1 m s^{-1}), is large.

To examine the radiative effects of aerosols and aqueous phase chemistry additional simulations have been done using the meteorological configuration in EXP3, with aerosol-radiation (wFB) feedback plus aqueous chemistry (wAq.chem), without aerosol-radiation feedback (nFB) but with aqueous chemistry, and without aqueous chemistry (noAq.chem) but with aerosol-radiation feedback. The analysis has been done for the fog events on 23rd and 24th December 2017 as

$$Impact\ of\ radiation\ feedback = Parameters\ in\ wFB - Parameters\ in\ nFB$$

$$Impact\ of\ aqueous\ phase\ chemistry = Parameters\ in\ wAq.chem - Parameters\ in\ noAq.chem$$

Emissions used in the WRF-Chem simulations are from the EDGAR-*HTAP v2 (Emissions Database for Global Atmospheric Research- Hemispheric Transport of Air Pollution;0.1° x 0.1°)* inventory for anthropogenic emissions and *FINN v2.2 (Fire INventory from NCAR; 1 km x 1 km) fire* emission inventory (Wiedinmyer et al., 2011). Trash-burning emissions (Chaudhary et al., 2021) are also included in the simulations. The model calculates the biogenic emissions online using MEGAN v2.04 (*Model of Emissions of Gases and Aerosols from Nature*) (Guenther et al., 2006). The initial and lateral boundary conditions for chemical constituents are from the global chemistry transport model CAM-Chem (*Community Atmosphere Model with Chemistry*) (Emmons et al., 2020).

The MOZART (Model for Ozone and Related chemical Tracers) chemical mechanism (Emmons et al., 2010) is used for gas-phase chemistry, which includes 85 gas-phase species, 39 photolysis, and 157 gas-phase reactions. It has been updated to include an explicit treatment of aromatic compounds, HONO, C_2H_2, and isoprene oxidation scheme (Knote et al., 2014). The lumped toluene used by Emmons et al., (2010) has been speciated into benzene, toluene, and lumped isomers of xylenes (Knote et al., 2014). For this study, HCl emissions, transport, dry, and wet deposition are represented. However, HCl gas-phase reaction is not included in MOZART.

The Model for Simulating Aerosol Interactions and Chemistry (MOSAIC) with four size bins (0.039–0.156, 0.156–0.625, 0.625–2.500, and 2.5–10.0 µm dry diameters) coupled with MOZART gas-phase chemistry is used (Fast et al., 2006; Zaveri et al., 2008). The bin sizes are defined by their lower and upper dry particle diameters, so there is no transfer of particles between bins during water uptake or loss. It is assumed that aerosols in each bin are internally mixed with the same chemical composition while they are externally mixed in different bins.

The aerosol composition includes sulfate (SO_4^{2-}), ammonium (NH_4^-), nitrate (NO_3^-), aerosol water, sea salt (Na^+, Cl^-), methanesulfonate (CH_3SO_3), carbonate (CO_3^{2-}), calcium (Ca^+), black carbon (BC), organic mass (OC), and unspecified inorganic species such as silica, inert minerals, and trace metals lumped together as other inorganic mass (OIN). For OC, primary OC and secondary OC are represented separately, where the latter is simulated using the volatility basis set (VBS) approach. Reactive inorganic species such as potassium (K^+) and magnesium (Mg^+) are usually present in much smaller amounts and are equivalent to Na^+ since their sulfate, nitrate, and chloride salts are similar in terms of their solubility in water.

218   MOSAIC treats condensation and evaporation of trace gases to/from particles, nucleation
219   (new particle formation), and coagulation. Aerosol coagulation (Brownian) is based on (Jacobson et
220   al., 1994) and nucleation is based on (Wexler et al., 1994) parameterization of H_2SO_4-H_2O
221   homogeneous nucleation. Sulfate, nitrate, chloride, and ammonium aerosols are mainly formed
222   through oxidation and neutralization/condensation of gas precursors. Gas-phase sulfuric acid (H_2SO_4)
223   is produced by the gas-phase oxidation of SO_2 by OH and nitric acid (HNO_3) formation is via the
224   oxidation of NO_2 by OH. HCl is a primary emission product. The neutralization/condensation of
225   H_2SO_4, HCl, and HNO_3 with NH_3 produces ammonium such as ammonium sulfate ((NH_4)$_2SO_4$),
226   ammonium bisulfate (NH_4HSO_4), ammonium chloride (NH_4Cl) and ammonium nitrate (NH_4NO_3),
227   respectively. The thermodynamic modules in MOSAIC for the dynamic gas-particle partitioning of
228   aerosols MTEM (Multicomponent Taylor Expansion Method) and MESA (Multicomponent
229   Equilibrium Solver for Aerosols) calculate the activity coefficient in aqueous phase aerosols and
230   compute the intraparticle solid-liquid phase equilibrium respectively (Zaveri et al., 2005, 2008). The
231   Adaptive Step Time-split Euler Method (ASTEM) coupled with MESA-MTEM dynamically
232   integrates the mass transfer equations.

233   Aqueous-phase chemistry uses a bulk water approach employing the Fahey and Pandis (2001)
234   mechanism. It calculates sulfate formation, formaldehyde oxidation, and non-reactive uptake of nitric
235   acid, hydrochloric acid, ammonia, and other trace gases (Chapman et al., 2009; Pye et al., 2020).
236   Aqueous-phase sulfate is produced via oxidation of SO_2 by H_2O_2, O_3, TMI (Transition metal Ion:
237   Fe(III), Mn(II)) catalyzed O_2 and NO_2. TMI concentrations are prescribed in the model to 0.01 $\mu g\ m^{-3}$
238   for Fe(III) and 0.005 $\mu g\ m^{-3}$ for Mn(II) (Martin and Good, 1991). The Fe(III) values are within the
239   range of water soluble iron in winter time aerosol reported in India (Kumar and Sarin, 2010). Wet
240   removal (scavenging), is represented by the (Neu and Prather, 2012) scheme for trace gases and Easter
241   et al., (2004) for aerosols.

242

243   **2.2 Observations**

244   To evaluate the model output, observations of aerosols and meteorology have been obtained
245   from several satellites as well as ground-based measurement platforms. To examine the aerosol
246   loading and spatial and temporal distribution, daily Level 2 Aerosol Optical Depth (AOD) retrievals
247   from the Moderate Resolution Imaging Spectroradiometer (MODIS) aboard Terra and Aqua satellites
248   are obtained at the spatial resolution of 10 km x 10 km (at nadir) pixel array. It provides aerosol
249   properties from the Dark Target (DT) algorithm applied over the ocean and dark land (e.g.,
250   vegetation) and Deep Blue (DB) algorithms over the entire land areas, including both dark and bright
251   surfaces. Each MOD04_L2 (Terra) / MYD04_L2 (Aqua) products are available at a 5-minute time
252   interval with an output grid of 135 pixels in width by 203 pixels in length.

253   The Indian National Satellites (INSAT-3D) in the geostationary orbit at inclinations of 82º

254 longitude provide an imager fog product (3DIMG_L2C_FOG) with a spatial resolution of 4 km every

255 30 min (www.mosdac.gov.in). For daytime, the visible channel observation is used to detect fog,

256 whereas thermal infrared is used to reduce false alarms such as medium/high clouds and snow areas.

257 INSAT 3D's 'day microphysics' data component analyzes solar reflectance at three wavelengths: 0.5

258 µm (visible), 1.6 µm (shortwave infrared), and 10.8 µm (thermal infrared). Night-time fog is derived

259 from TIR-1 (12.0 µm and 10.0 µm) and MIR (10.8 µm and 3.9 µm) channel brightness temperature

260 over the Indian region. INSAT-3D provides fog intensity varying from 1 to 4 indicating SHALLOW

261 for visibility > 600 m; MODERATE, DENSE, and VERY_DENSE, respectively for visibility varying

262 from 0 to 500 m (Banerjee and Padmakumari, 2020). If the visibility is greater than 700 m it indicates

263 no fog while visibility > 1000 m represents very clear skies. Validation of INSAT-3D fog products

264 over the IGP shows a 66%-68% probability of detection and a 10% false alarm rate. It also captures

265 the entire life cycle of fog from formation to dissipation. However, detecting fog during multilayer

266 clouds is still challenging with INSAT-3D (Arun et al., 2018; Chaurasia and Gohil, 2015; Chaurasia

267 and Jenamani, 2017).

268   Ground-based monitoring sites provide hourly data of relative humidity, surface temperature,

269 and wind speed measured by the Central Pollution Control Board, CPCB (http://cpcb.nic.in). Given

270 the data availability from CPCB stations, nine stations have been considered representing each region

271 of IGP, which include, Amritsar, IGI Airport (Indira Gandhi International Airport, Delhi), IHBAS

272 (Delhi), Dwarka (Delhi), RKP (Delhi) in the North-West IGP; Kanpur, Lucknow in Central IGP and

273 Patna, Muzaffarpur in East IGP.

274   In addition, measurements of several aerosols, trace gases, and meteorology at Delhi (IGI

275 Airport) from the Winter Fog Experiment (WiFEX) for the period December 10-31, 2017, have also

276 been used to validate the model output. The WiFEX, an initiative of the Ministry of Earth Sciences

277 (MoES), India, is a ground-based measurement campaign at the IGI Airport Delhi to understand fog's

278 physical and chemical features. Additional details of the WiFEX project and related publications can

279 be found in Ghude et al., (2017).

280

281   **3**   **Meteorology Evaluation**

282   Previous studies simulating fog highlight the importance of high model vertical resolution

283 (Pithani et al., 2019; Van Der Velde et al., 2010) for representing the fog formation and the growth of

284 the fog layer, model initialization (Yadav et al., 2022), initial relative humidity (Bergot and Guedalia,

285 1994; Pithani et al., 2020), and PBL schemes (Chen et al., 2020; Pithani et al., 2019). In the present

286 study, 2-m relative humidity (RH2), 2-m temperature (T2), and 10-m wind speed (WS) from WRF-

287 Chem have been evaluated using ground-based measurements from CPCB monitoring network and

288 WIFEX campaign for nine stations across the IGP. The comparison of WRF-Chem results with

289 observations shows that RH2 and T2 are sensitive to the choice of the meteorological initial and

290 boundary conditions as illustrated by six stations in major cities (Fig. S1). WRF-Chem compares
291 better with the observations for simulations driven by the ERA-Interim reanalysis than with GFS-FNL
292 reanalysis since ERA-Interim provides more realistic RH2 than GFS-FNL (Figs. S2 a-f). For example,
293 RH2 from EXP1 (GFS) varies from 10 to 50%, while RH2 from EXP2 and EXP3 varies from 30 to
294 100%, which is closer to observation, especially for NWIGP and CIGP. For EIGP, RH2 from EXP1
295 (GFS) compares better than ERA-Interim, which overestimates the observed RH2. ERA-Interim and
296 YSU PBL scheme showed damping of RH2 continuously increasing the bias in RH2 with time (not
297 shown), which was corrected in EXP2 by refreshing meteorology every day at 00h UT during the
298 model simulation. In addition, maps of surface RH2 and T2 (Figs. S2 g-j) show that the GFS-FNL
299 dataset has lower relative humidity throughout the domain as compared to ERA-Interim. There are
300 differences in simulated 2-m temperature between these two datasets which are of smaller relative
301 magnitude compared to the RH2.

302 The GFS-FNL driven meteorology EXP1 has a warm bias in NWIGP and CIGP, especially during
303 night-time, while over EIGP, the model prediction agrees well with observations. EXP2 with the
304 ERA-Interim driven meteorology and YSU PBL scheme also shows good agreement between
305 modeled and observed T2 in EIGP. The ERA-Interim driven meteorology with the ACM2 PBL
306 scheme in EXP3 has a cold bias of up to 7ºC over EIGP during daytime from 22nd to 24th December.
307 The wind speed evaluation shows that WRF-Chem is over-predicting wind speed. However, it is also
308 possible that some CPCB stations (e.g., Amritsar and RK Puram) have a wind speed low bias due to
309 the low measurement height and obstructions such as tall trees near the monitoring station as shown in
310 FigS3. WRF-chem in general overestimates wind speed and several earlier studies have reported this
311 bias in wind speed (e.g., Mohan and Gupta 2018; Pithani et al.,2019). Moreover, WRF-Chem does not
312 have the capability to represent building meteorology and parameterizes the effects of urban areas on
313 meteorology through roughness length, which likely leads to overestimation of wind speed. Note that
314 at other sites (e.g., over IGI-Delhi and Kanpur) the model measurement agreement is better.

315   The WRF-Chem performance has been statistically assessed against observation using the
316 Taylor Diagram (Taylor, 2001), which provides a statistical summary of how well the model output
317 agrees with the observation in terms of the Pearson correlation, their centered root-mean-square error
318 (RMSE) difference, and the ratios of their variances (Fig. 2).

319 The centered RMS difference, the correlation, and the standard deviation are related by the following
320 formula:

321 $E'^{2} = \sigma_o^2 + \sigma_m^2 - 2\sigma_o\sigma_m R$

322 where R is the correlation coefficient between the model-simulated and observed fields, E' is the
323 centered RMS difference between the fields, and σ_m^2 and σ_o^2 are the variances of the model-simulated
324 and observed fields, respectively. The correlation(R), centered RMS difference (E') and standard
325 deviations of the model simulated and observed fields are calculated by the following formulas:

326 $$R = \frac{\frac{1}{N}\sum(M_n - \bar{M})(O_n - \bar{O})}{\sigma_m \sigma_o}$$ (1)

327 $$E'^2 = \frac{1}{N}\sum[(M_n - \bar{M}) - (O_n - \bar{O})]^2$$ (2)

328 $$\sigma_m{}^2 = \frac{1}{N}\sum(M_n - \bar{M})^2$$ (3)

329 $$\sigma_o{}^2 = \frac{1}{N}\sum(O_n - \bar{O})^2$$ (4)

330 where the overall mean of a field is indicated by an overbar.

331   The percentage bias has also been included to further evaluate the WRF-Chem results. In Fig.

332 2, better agreement of WRF-Chem results with observations are shown by the marker's proximity to

333 the "OBS" dashed black line. The WRF-Chem RH has a good correlation for all three experiments

334 with r > 0.75 at all the locations in IGP for all the experiments. However, the RMSE (shown by red

335 dashed contours) and the standard deviations are larger for the EXP1. The relative bias is also large

336 (>20%) for EXP1 (GFS-FNL) compared to EXP2 and EXP3 which lie closer to the dashed black line

337 indicating that the simulated RH variations are similar to observations. For all the experiments, WRF-

338 Chem T2 agrees well with observations with a correlation between 0.8 and 0.95. The points are

339 concentrated near the dashed line showing a low RMSE and standard deviation for T2, signifying a

340 good agreement of simulated T2 with observation in terms of temporal variation but the T2 relative

341 bias is large for EXP1 (>20%). The RMSE and relative bias for EXP1 are larger for several of the

342 stations. The temporal variability of T2 and RH is predicted well for all the combinations of inputs

343 (Fig. S1), however, the accuracy of simulated T2 and RH is sensitive to the choice of meteorological

344 initial/boundary conditions. WRF-Chem predicted RH and T2 agree better with observations when

345 initialized with ERA-Interim meteorology than with GFS-FNL.

346   The WRF-Chem runs driven by ERA-Interim with YSU (EXP2) and ACM2 PBL (EXP3)

347 schemes predicted the surface meteorology better over the IGP than the WRF-Chem run driven by

348 GFS (EXP1). By examining the modeled cloud water content in the lowest model level with the

349 INSAT-3D satellite fog intensity for the 23rd and 24th December 2017 (Fig. 3), it is apparent that

350 WRF-Chem with the ACM2 PBL scheme compared qualitatively well with observations obtained

351 from INSAT-3D satellite in terms of fog coverage over CIGP, while the WRF-Chem run with the

352 YSU PBL scheme did not produce widespread fog. However, there is also fog over EIGP in WRF-

353 Chem with the ACM2 PBL scheme although it is not observed by the satellite. This is because the

354 model has a cold bias in T2 and a high surface RH over East IGP with ACM2 PBL and Pleim-Xiu

355 surface scheme as discussed earlier, which favors the formation of fog in this region. The time series

356 in Fig. 4 shows that EXP3 is capable of predicting the duration of fog on 23rd and 24th December.

357 There is a data gap from INSAT 3D observations because it is unable to capture fog during daytime in

358 the presence of mid and high-level clouds.

359   In conclusion, EXP3 is the best configuration for predicting fog formation where the ERA-

360 Interim meteorology, the ACM2 PBL and surface schemes, and soil moisture nudging is used in the

WRF-Chem simulation. Therefore, the evaluation of predicting AOD, surface aerosol concentrations, and aerosol composition as well as analysis of the impact of aerosols on fog formation uses the EXP3 configuration.

4   Aerosol Evaluation

Aerosol is an important factor in correct prediction of fog (Maalick et al., 2016; Stolaki et al., 2015) as the number of fog droplets depends on the aerosol size distribution and concentration. Aerosols as CCN can affect the liquid water content in fog and therefore an increase in aerosol concentration can significantly affect fog lifetime (Stolaki et al., 2015; Zhang et al., 2014b). AOD retrievals from the MODIS satellite have been used to validate the modeled AOD (Fig. 5). It is observed that the model captures several important features of the MODIS retrieved AOD spatial distribution but at the same time somewhat struggles to reproduce the observed AOD magnitude in some parts of the domain. One possible reason for the underestimation would be the EDGAR-HTAP emission inventory, which has a low bias for residential sector $PM_{2.5}$ emissions in India (Sharma et al., 2022). For instance, the model successfully predicts high aerosol loading seen by MODIS on 20 and 21 December over CIGP and EIGP. This is the region with dense fog both in model and observation. Higher AOD (>0.5) over CIGP and EIGP can be attributed to the accumulation of aerosols that are transported by north-westerly winds to these regions from NWIGP (Dey and Di Girolamo, 2011; Jain et al., 2020; Jethva et al., 2018; Kumar et al., 2018; Yadav et al., 2020). However, WRF-Chem underestimates AOD over the NWIGP (AOD<0.3) throughout the simulation period and during 23-24 December over CIGP and EIGP where the latter may be related to enhanced scavenging of aerosols by fog droplets.

The west to east gradient in aerosol loading over IGP is consistent with surface $PM_{2.5}$ distribution (Fig. 6a). Surface $PM_{2.5}$ concentration is highest in EIGP (>100 µg/m^3) and it decreases gradually towards NWIGP (~60-80 µg/m^3). The time series of $PM_{2.5}$ from CPCB measurements and the model at stations representative of each region in IGP shows that simulated $PM_{2.5}$ compares well with observation in terms of day-to-day variation over most of the locations in the IGP (Fig. 6 b-e). The comparison is good over Amritsar (an NWIGP location), where $PM_{2.5}$ is mostly primary aerosols from local emissions e.g., residential heating related biomass burning. Agricultural waste burning is at its peak during post monsoon months (Oct-Nov), whereas during winter burning for residential heating increases and the stable boundary layer confines these emissions near the surface (Kumar et al., 2021; Pawar and Sinha, 2022). $PM_{2.5}$ at Amritsar shows a bimodal distribution with morning and evening peaks whereas it is absent in the model likely due to the absence of diurnal variations in the WRF-Chem anthropogenic emissions.

A statistical analysis (Table S1) shows a minimum mean bias for $PM_{2.5}$ at Amritsar (-2.2%) while in other stations it ranges from 48 to 53% similar to the reported range of model bias (underestimated by 40–60%) in winter over IGP by earlier studies (Bran and Srivastava, 2017; Ojha et al., 2020). RMSE

values range from 41 to 138 µg/m^3 (normalized RMSE~0.4 to 0.7) comparable to the reported values by these studies. The Pearson correlation coefficient (r) for the simulated and observed day-to-day variation in PM$_{2.5}$ lies between 0.4 and 0.7 for all the stations in Fig. 6 except at Patna which lies within the range in these studies. Poor correlation at Patna is due to the loss of PM$_{2.5}$ during fog in the model as discussed earlier.

At Delhi, the daily variations are predicted well although WRF-Chem underestimates PM$_{2.5}$ observations during the first 4 days. Delhi experiences severe air pollution and haze with high PM loading (> 500 µg m^{-3}) (Bharali et al., 2019). The model is successful in predicting the high PM$_{2.5}$ episode on the 24th of December, but WRF-Chem underpredicts the SO$_4^{2-}$, NH$_4^+$, NO$_3^-$ and Cl$^-$ concentrations (Fig. 7). Although simulated SO$_2$ and NH$_3$ are comparable with observation, sulfate, and ammonium are underestimated in the model. SO$_4^{2-}$ is underestimated by ~ 9 µg m^{-3}, while NH$_4^+$, NO$_3^-$ and Cl$^-$ are underestimated by ~30 µg m^{-3}, ~19 µg/m^3 and ~40 µg/m^3 on average, respectively. In addition, the WRF-Chem model results show that a large percentage of PM$_{2.5}$ is classified as "other inorganics", which is usually dominated by PM$_{2.5}$ other than BC and OC. This leads to the underestimation of PM$_{2.5}$ over Delhi. Studies report very high chloride over the IGP with values exceeding 100 µg m^{-3} (Lalchandani et al., 2021) during winter emitted from increased trash burning and industrial emissions (Pant et al., 2015; Patil et al., 2013). WRFChem incorporates trash-burning emissions which include HCl emissions from Chaudhury et al., (2021) for this study however, the inventory contains annual emissions and fails to resolve the seasonality of trash-burning emissions as identified by Nagpure et al., (2015). They suggested almost all the waste-burning emissions in neighbourhoods with higher socioeconomic status in Delhi occur due to the use of waste as cheap heating fuel by individuals such as night watchmen and pavement dwellers. Chaudhary et al., (2021) considers waste burning that occurs due to lack of collection infrastructure, and at landfills and, therefore, shows a concentration of waste burning emissions around the periphery of Delhi but low waste burning emissions in the relatively prosperous city centre. In addition, emissions from other sources (e.g., industries) are unaccounted for in the model which likely leads to the underestimation in modeled chloride.

Over the CIGP and EIGP, the underestimation in PM$_{2.5}$ is mostly observed at the east IGP locations during the dense fog. It is well known that the hygroscopic aerosols grow in size and are deposited to the surface during fog (Gupta and Mandariya, 2013; Kaul et al., 2011). PM$_{2.5}$ shows an increase initially with the onset of fog and then it decreases as the aerosols grow and get deposited through fog droplets. A two order higher deposition rate (Fig. 6 f, g) during fog compared to the deposition rate of dry aerosol results in the lower PM$_{2.5}$ over CIGP and EICP during fog events.

Previous studies have reported that models tend to underestimate the AOD observation (David et al., 2018; Pan et al., 2015) during the post-monsoon and winter when agricultural waste burning and anthropogenic emissions dominate. While anthropogenic emissions include a contribution from the residential sector, the emissions from small-scale burning for residential heating over IGP especially

during winter are likely underestimated in the current emission inventory (Sharma et al., 2022). This leads to an underestimation of aerosol concentration in the model. Other possible causes for the underestimation are the biases in the simulated meteorology (Govardhan et al., 2015; Kumar et al., 2015; Pan et al., 2015) which affects the aerosol concentration. We corrected some of the biases in meteorology as discussed earlier however there are still residual biases in the simulated meteorology e.g., overestimation of wind speed by WRF-Chem. We also observe underestimation of secondary aerosols over NWIGP which contribute significantly to the aerosol loading over IGP. Secondary aerosol formation is substantial over CIGP and EIGP in the model compared to NWIGP which will be discussed in a later section. The underestimation of PM$_{2.5}$ could also be linked to the uncertainty in the model's chemistry scheme to simulate the secondary aerosols due to missing chemical processes or due to underestimation of sulfur oxidation at different RH levels (Acharja et al., 2022; Pawar et al., 2023; Ruan et al., 2022) . Moreover, several modeling studies have shown significant improvements in forecasting surface PM$_{2.5}$ by assimilation of satellite AOD and PM$_{2.5}$ (Ghude et al., 2020; Jena et al., 2020; Kumar et al., 2020) suggesting the importance of correct initialization of the model in simulating aerosols over IGP.

5   Effect of Aerosol Radiation feedback

Interactions of aerosols with radiation affects temperature and surface heat fluxes, thereby weakening the turbulence in the PBL and stabilizing the boundary layer height (Fig. 8b) compared to the clean environment (Fig. 8a). In the presence of well mixed aerosols within the PBL, the radiative effect of aerosols lowers the noontime PBL height (Fig. 8b). However, the presence of absorbing aerosols in the PBL warms the air and changes the thermodynamics. Three cases are shown in Fig. 8(c-e) where increases of scattering aerosol concentrations at the top of PBL (Fig. 8c) increases scattering of radiation by the aerosol layer and reduces the surface reaching solar radiation similar to Fig. 8b. Higher concentrations of absorbing aerosols at the top of PBL (Fig. 8d) warms the air above the boundary layer and strengthens the capping inversion stabilizing the PBL and suppressing its growth. The shallow PBL and weakened daytime vertical mixing confines aerosols and water vapor near the surface and worsens the air quality of a region. The aerosols trapped in the stagnant PBL further affects the radiation flux at the surface and creates a positive feedback loop wherein the PBL is continually suppressed until interrupted by some synoptic weather phenomenon, such as the western disturbances in the IGP. On the other hand, higher concentration of absorbing aerosols within the PBL (Fig. 8e) warms the air in the PBL and this results in the higher PBL height. The raised PBL decreases the aerosol concentration near the surface which is termed as a negative feedback effect.

The aerosol radiation feedback can affect shortwave heating rates (SWHR). The high aerosol loading over the IGP (Fig. 6 and Fig. 7) allows the AR feedback to reduce the PBL height by more than 140 m throughout the IGP compared to the surrounding region with AR feedback (Fig. 9a). The difference in PBL height with and without aerosol radiation feedback is largest during noontime. The

472 suppressed PBL is due to the decrease in the surface heating flux and the consequent weakening of

473 turbulence in the PBL. The surface solar radiation flux (SWF) decreases by 5-35 % while the surface

474 latent heat (LH) and sensible heat (HFX) fluxes decrease by 5-35 % and 10-60 %, respectively (Fig.

475 S3). The stable, shallow PBL reduces the vertical mixing of aerosols and moisture and confines them

476 near the surface, resulting in increased $PM_{2.5}$ concentrations and RH near the surface with AR

477 feedback (Fig. 9). Although T2 should decrease with the reduction in surface SWF, T2 shows mixed

478 signals with both cooling and warming over IGP. While surface cooling is observed over NWIGP and

479 EIGP, T2 increases with AR feedback over most of CIGP. The response of AR feedback to T2 varies

480 in these three regions probably due to differences in the distribution and types of aerosols and the

481 presence of fog. Increase in surface concentration of $PM_{2.5}$ occurs more over NWIGP and EIGP with

482 increase in BC and OIN over NWIGP, and sulfate aerosol over EIGP which results in the surface

483 cooling due to positive AR feedback in these two regions. Over the CIGP, the AR feedback causes a

484 depletion of surface $PM_{2.5}$ (Fig. 9d), which is likely due to their hygroscopic growth, and then dry

485 deposition (average dry deposition flux of $PM_{2.5}$=331 $\mu g/m^2/hr$ with AR feedback and 282 $\mu g/m^2/hr$

486 without AR feedback) in dense fog. The increase in RH with AR feedback favours the growth of

487 aerosols in size by the uptake of water

488   Examining further, the time variation of the changes in PBL height, T2, and RH between the

489 simulations with and without aerosol-radiation feedback (Fig. 9g) shows an increase in T2 while the

490 surface fluxes, sensible heat flux, latent heat flux, and downward shortwave radiation flux decrease

491 over CIGP (Fig. 9h). AR feedback affects mostly the lower atmosphere at multiple levels; however,

492 our finding suggests that the decreased shortwave radiation flux decreases the surface fluxes and thus

493 the turbulence in the boundary layer resulting in a reduced PBL height on both days. Figure 9 g and h

494 clearly show a decrease in HFX and LH following the decrease in SWF. Moreover, we observe that

495 the PBL height is sensitive to latent heat flux likely due to its strong dependence on moisture

496 availability (Xiu and Pleim, 2001; Zhang and Anthes, 1982).

497   The impact of AR feedback on T2 depends on factors such as the presence of absorbing

498 aerosols and their vertical distribution via heating or increased SWF (as observed in CIGP, Fig. S4).

499 Absorbing aerosols in WRF-Chem include BC and OIN (other inorganic aerosols), which both

500 increase near the surface (Fig. 9e, Fig. S5) due to their confinement in the stable PBL. Some areas in

501 the fog-affected region show a decrease in BC as well as SO_4^{2-} likely due to increased dry deposition

502 in fog water as discussed earlier in this section for $PM_{2.5}$ As a result, AR feedback changes the

503 absorbing to scattering ratio of aerosols over IGP indicated by the decrease in SSA (Single Scattering

504 Albedo; Fig. S6). In EIGP, sulfate concentrations is larger with AR feedback than without AR

505 feedback with time periods where the difference is >1 $\mu g/m^3$ (Fig.11). The BC concentration changes

506 are small (<0.5 $\mu g/m3$) in the EIGP, resulting in a higher SSA near the surface with AR feedback in

507 EIGP. In the CIGP, BC concentrations increase while sulfate aerosols decrease within the PBL with

508 AR feedback (Fig.11) compared to the simulation without AR feedback. A decrease in SSA is seen for

the CIGP throughout the boundary layer while in EIGP the decrease occurs near the top of the PBL; difference in SSA due to AR feedback is negligible in NWIGP. Also contributing to the higher SSA in EIGP is the increase in RH (Fig. 9) due to AR feedback favoring the growth of aerosols in size by uptake of water and the production of secondary aerosols such as SO_4^{2-} and NH_4^+.

A similar observation has been made by Ramachandran et al., (2020) where SSA decreases with increasing altitude due to absorbing carbonaceous aerosols at higher elevations which contributes ≥75% to the aerosol absorption over IGP. Increased shortwave heating (Fig. 10) is probably caused by the increased absorbing aerosols near the surface which overwhelms the surface cooling due to reduced shortwave radiation at the surface.

The increase in 2-m RH is substantial over CIGP on 24th December (Fig. 9g) compared to the previous day following the decrease in PBL height which constrains the moisture near the surface. The decrease in RH by 2% or more when aerosol-radiation feedback is included compared to no aerosol-radiation feedback is likely due to increase in T2. However, the increase in RH in the afternoon associated with a decrease in LH and PBL height is important for the air to saturate which then favors the formation of fog in a polluted environment. Note that the increase in T2 with AR feedback is very small (<0.5°C) which reduces further after noon (~12:30 pm IST) on both days.

Another important factor that can affect the extent of change in PBL height is the distribution of aerosols in the vertical (illustrated in Fig. 8). The pressure-time cross-sections of differences in T, $PM_{2.5}$, BC, and SO_4^{2-} between aerosol radiation (AR) feedback (wFB) and no aerosol radiation feedback (nFB) for three regions, NWIGP, CIGP, and EIGP are shown in Fig. 11. The difference in the PBL height reaches a maximum with the AR feedback during midday (12:30-15:30 IST). Increase in temperature in the boundary layer is observed with AR feedback particularly at the upper PBL in all the regions of IGP. This induces a temperature inversion resulting in a stable and suppressed PBL. In all the regions the decrease in PBL height (100-200 m) is larger on 24th December compared to 23rd December. The difference in the PBL height on 23rd and 24th December with AR feedback on these days is possibly controlled by the aerosol distribution during the previous day or early morning on the same day. For example, in all the regions an increase in $PM_{2.5}$ is observed the previous night (23:30 onwards) till ~11:30 of December 24, with increased BC over NWIGP and CIGP whereas both BC and SO_4^{2-} over EIGP. The increased $PM_{2.5}$ concentrations suppress the development of the PBL after sunrise with AR feedback on December 24 compared to that on December 23, leading to the observed differences in ΔPBL height on these two days. Increase in BC concentrations in NWIGP and CIGP are found above the PBL on 24th December whereas BC concentrations decrease within the PBL. This BC concentration gradient creates a temperature inversion, for example between 10:30-14:30 IST. The increase in BC warms the air in the PBL; however, the warming is not strong enough to cause negative feedback over CIGP. On 23rd December a small increase in BC is uniform throughout the PBL, while there is a decrease in SO_4^{2-} concentrations, resulting in a warmer PBL (Fig. 11) with AR feedback.

In EIGP, BC distribution is similar to that in CIGP with AR feedback while there is a substantial increase in sulfate aerosol in the PBL. This results in the strongest extinction in EIGP as evident from the largest difference in PBL height and surface cooling with AR feedback among the three regions. Although ΔPBL is small on 23rd December, it still results in the accumulation of aerosols during night-time (~23:30 pm onwards) which further strengthens the AR feedback effect the next day in NWIGP and CIGP. Thus, AR feedback stabilizes the PBL, increases PM$_{2.5}$ and RH in the PBL making conditions favourable for persistence of fog over IGP.

6   Effect of Aqueous phase chemistry

In this section we discuss the impact of aqueous phase chemistry on aerosol composition and its interaction with meteorology. There is a considerable difference in the surface concentration of PM$_{2.5}$ (>16 µg m^{-3}) in the absence of aqueous chemistry over CIGP and EIGP where fog occurs (Fig. 12a) while the difference is negligible over NWIGP where fog does not occur. This is due to the formation of secondary aerosols through aqueous phase chemistry and the hygroscopic growth of aerosols during fog in these regions with the inclusion of aqueous chemistry in the model. In the region between CIGP and EIGP (83E-84E; marked by the box in Fig. 12a), PM$_{2.5}$ concentration is less in the simulation with aqueous-phase chemistry than without aqueous-phase chemistry because deposition of fog water aerosols to the surface increases as the fog thickens (Fig. 13, Fig. S7). Figure 13 shows the relation between formation of secondary aerosols, deposition flux of PM$_{2.5}$, and fog with and without aqueous phase chemistry. During the fog event, the secondary aerosols (SO$_4^{2-}$, NH$_4^+$) increase significantly by 4-10 µg m^{-3} due to aqueous phase chemistry adding to the PM$_{2.5}$ burden over IGP. The intensity of fog is high around midnight December 24-25 compared to that on 23rd and 24th (1:30-11:30 IST)) which increases the dry deposition flux of PM$_{2.5}$ causing a sharp drop in the PM$_{2.5}$ concentration on 24th December compared to the previous night's fog event. The observed change in PM$_{2.5}$ over a region is the net result of the formation of secondary aerosols and its deposition with fog droplets.

The composition distribution of PM$_{2.5}$ (Fig. 12b) has a similar distribution for the simulations with and without aqueous phase chemistry over NWIGP where fog did not occur. The primary aerosols are higher (BC > 9%, OC ~ 16-30%, OIN > 50%), than the secondary aerosols (<5%). While the model requires fog for accelerated formation of secondary inorganic aerosol, experimental data (Fig. 7) supports significant formation of secondary inorganic aerosol at elevated RH levels even in haze aerosol (Acharja et al., 2022). On the other hand, the central and east IGP stations are fog-covered and therefore, there is an increase in secondary aerosols especially SO$_4^{2-}$ and NH$_4^+$ when aqueous phase chemistry is included in the simulation. SO$_4^{2-}$ is chemically produced via aqueous phase chemistry in cloud water, hence the abrupt increase whereas NH$_4^+$ maintains a gas-aerosol and gas-cloud equilibrium with NH$_3$ and SO$_4^{2-}$ via neutralizing the drop or aerosol. NO$_3^-$ is high in the model compared to SO$_4^{2-}$ and NH$_4^+$ and it decreases by ~1-2 % with aqueous phase chemistry. We

583 observe a small increase in NO_3^- during fog, however it drops as fog intensifies, more rapidly than that

584 without aqueous phase chemistry likely due to increase in dry deposition. This results in lower

585 average NO_3^- to $PM_{2.5}$ ratio with aqueous phase chemistry. Moreover, NO_3^- is high over the fog

586 covered CIGP and EIGP compared to NWIGP suggesting that transport and chemistry of NO_x in

587 CIGP and EIGP produce more HNO_3. Aerosol NO_3^- is also in equilibrium with HNO_3 and it is formed

588 only if excess NH_3 is available beyond the sulfate neutralization. Thus, NH_4^+ and NO_3^- changes are

589 likely due to changing the partitioning between gas and liquid based on the production of sulfate.

590         $PM_{2.5}$ is mostly composed of organic aerosols (OA) over CIGP and EIGP (Lalchandani et al.,

591 2021; Srinivas and Sarin, 2014) whereas $PM_{2.5}$ is OIN (dust) and OA over NWIGP (Ram et al., 2012a;

592 Sharma and Mandal 2023). Although observational studies report Cl^- as one of the largest contributors

593 (12-17%) to $PM_{2.5}$ after the organics (Lalchandani et al., 2021; Pant et al., 2015) during winter, Cl^- is

594 largely underestimated by the model as discussed in section 4 and contributes only ~3%. A small

595 increase (2-4%) in secondary organic aerosols (SOA) from glyoxal production in aerosols occurs for

596 the simulation with aqueous phase chemistry included during intense fog, suggesting there are

597 feedbacks between cloud chemistry (without glyoxal aqueous chemistry) and aerosol chemistry.

598 However, similar to NO_3^-, average SOA (ASOA (anthropogenic)+BSOA (biogenic) + GlySOA)

599 shows a decrease when aqueous phase chemistry is included. SOA contributes significantly to organic

600 aerosol loading over IGP (Kaul et al., 2011; Mandariya et al., 2019).

601   The WRF-Chem results on aerosol composition during fog behave similarly to observational

602 studies. For example, Ram et al., (2012a) reported an increase of EC, OC, and WSOC concentrations

603 by ~30% during fog and haze events at Allahabad, a location in the Central IGP, and a marginal

604 increase of these constituents at Hisar (NWIGP). Several studies report an increase in inorganic ions

605 (NH_4^+, NO_3^-, and SO_4^{2-}) during fog over IGP and elsewhere (Gundel et al., 1994; Ram et al., 2012a).

606 Recent studies suggest that a significant fraction of atmospheric particulate matter in the IGP is

607 comprised of carbonaceous aerosol (~30–35% of the PM) and water-soluble inorganic species (~10–

608 20% of the PM) during October−January when emissions from biomass burning (including residential

609 heating) are dominant over IGP (Ram et al.,2012b; Rengarajan et al., 2007; Tare et al., 2006).

610   Both the simulations with and without aqueous-phase chemistry include the AR feedback. The

611 aqueous chemistry increases the mass of $PM_{2.5}$ and the size of the aerosols, both of which contribute to

612 AR feedback, thus increasing RH and PBL stability. The increase in RH also saturates the air,

613 promotes aerosol growth by water uptake, and thus favors fog formation. Since the secondary

614 inorganic aerosols are scattering aerosols, the increased scattering of radiation further reduces the

615 solar radiation reaching the surface (Fig. 14a). Over CIGP the presence of higher aerosol loading

616 reduces the T2 during daytime, particularly on the 24th of December which then reduces the PBL

617 height and increases RH near the surface (Fig. 14b). These conditions favor fog formation over the

618 CIGP. Further, the fog water content with aqueous-phase chemistry is higher than that without

619 aqueous-phase chemistry on 24th December post-midnight (Fig. 13b). This is likely due to saturation

620 of air due to increase in RH and lower T2, induced by the AR feedback caused by the increase in

621 $PM_{2.5.}$ Although the difference in T2 is small (<0.4), favourable conditions mentioned above are

622 conducive to fog formation. Because aqueous chemistry increases sulfate concentrations, the size of

623 the aerosols also increase. The increased aerosol size, which can grow further by water uptake, also

624 impacts the solar radiation reaching the surface, affecting fog formation and dissipation.

625

626 ## 7   Effect of AR feedback and aqueous chemistry on the duration of fog

627 Aerosol and its radiative effects impact fog characteristics, including the fog liquid water content

628 (LWC), the fog lifetime over a region and hence its spatial and temporal distribution. Variations of fog

629 LWC in WRF-Chem contrast the fog in the CIGP and EIGP (Figure 15) as well as among the three

630 experiments (with aqueous chemistry plus AR feedback, with aqueous chemistry without AR

631 feedback, and without aqueous chemistry but with AR feedback). WRF-Chem does not simulate fog

632 over NWIGP in the model for the study period. In Figure 15, only foggy grid points are considered for

633 the first fog event on 23-24 December. The LWC is 5-15% higher with AR feedback than without AR

634 feedback and without aqueous phase chemistry for both CIGP and EIGP. The interquartile range is

635 larger for the simulation with and without AR feedback than without aqueous phase chemistry in

636 CIGP showing large variability in the LWC. On the other hand, in EIGP the variability in LWC is

637 greater in the simulation with AR feedback compared to the other two experiments.

638   The formation and dissipation times of the two fog events for the three experiments are listed

639 in Tables 2 and 3 for CIGP and EIGP. The 23-24 December fog starts forming two hours earlier and

640 the 24-25 December fog forms one hour earlier in both CIGP and EIGP with AR feedback than

641 without AR feedback. In the simulation without aqueous phase chemistry, fog formation is delayed by

642 an hour or two compared to the simulation with aqueous chemistry plus AR feedback in CIGP. In

643 EIGP the 23-24 December fog forms at the same time with AR feedback and without aqueous phase

644 chemistry while the 24-25 December fog is delayed by an hour without aqueous phase chemistry. Fog

645 dissipation usually occurs after sunrise when the shortwave radiative warming at the surface warms

646 the air, which results in PBL mixing. In addition, absorbing aerosols like BC affect fog dissipation by

647 increasing the radiative heating in and above the fog. We find an increase in BC and shortwave

648 heating in the PBL with AR feedback (Fig. 10,11) and warming over CIGP with AR feedback. Fog

649 intensity starts to decrease after 01:00 UTC (06:30 IST), however, in our study, we find that the fog

650 dissipates completely in the afternoon (~10:00 UTC or 15:30 IST) for both the simulations with AR

651 feedback and no aqueous chemistry while an hour later without AR feedback in CIGP. Fog dissipation

652 is delayed in EIGP with AR feedback compared to that without AR feedback and without aqueous

653 phase chemistry. In both the regions, fog lifetime increases with AR feedback. All the stations,

654 however do not show the same pattern, for example, the 23-24 December fog in Lucknow forms and

655 dissipates at the same time for simulations with AR feedback and without aqueous phase chemistry,

656 and the 24-25 December fog forms later with AR feedback than without AR feedback. Patna shows no

difference in the 24-25 December fog formation in all the three experiments. To gain better insights on the fog timing, we recommend that simulations at higher spatial and temporal resolutions be performed to represent better the fog dynamics at point locations. Furthermore, there are other important factors to consider, e.g., improved emissions, better simulations of aerosol chemical composition, and evaluation of aerosol deposition.

The AR feedback and aqueous-phase chemistry have the potential to impact aerosol-fog interactions. We can learn about the effect of the aerosol-radiation interactions on CCN concentrations because the WRF-Chem model calculates the CCN concentrations at different supersaturations as a diagnostic output. We compare CCN at 0.02% supersaturations, a value typical of fog, among the three experiments. For the 23-24 December fog in CIGP, hourly CCN concentrations are ~10% higher for the simulations with AR feedback with or without aqueous chemistry than with no AR feedback (Figure S8) during the first 8 hours of the fog event (16:00-24:00 IST 23 December). Surprisingly, the simulation with no aqueous chemistry has higher CCN concentrations than the simulation with aqueous chemistry, as more CCN are expected with aqueous chemistry. However, the dry deposition flux (ddmass) also increases in dense fog which causes rapid loss in CCN and activated aerosols during fog events with the AR feedback (Fig. S7) and more so without aqueous-phase chemistry. Shao et al. (2023) examined aerosol-fog interactions for two consecutive fog events by comparing WRF-Chem results with current emissions strengths to those with low emission strengths. They show that the first fog event promotes formation of the second fog event leading to wider fog distribution, and longer fog lifetime favoured by multiple feedbacks including AR feedback i.e., low temperature, high humidity and high stability similar to our study. While Shao et al. (2023) observe a delay in dissipation of the first event and early formation of second fog event, we find an early dissipation and early formation of fog with AR feedback as discussed earlier in this section. In summary, aqueous phase chemistry together with AR feedback promotes early formation of fog while AR feedback alone promotes early dissipation of fog and plays a critical role in the formation and evolution of the fog over IGP.

8 Conclusions

The effects of aerosol-radiation (AR) feedback and aqueous chemistry in air quality and fog have been assessed over IGP. We carried out three experiments using WRF-Chem testing different combinations of PBL schemes and meteorology initial and boundary conditions. The best representation of surface meteorology for the IGP region for the case study (December 20-24, 2017) used ERA-Interim reanalysis to drive the meteorology and ACM2 PBL scheme with soil moisture nudging to ERA-Interim. With this meteorology configuration for WRF-Chem, evaluation of aerosol concentrations with measurements and the impact of aerosols on atmospheric processes during fog were examined. Further, we included trash-burning emissions to represent anthropogenic chloride aerosols in our configuration. Incorporation of trash burning emissions did improve the model

694   simulations of PM$_{2.5}$ and better captured the day-to-day variability of PM$_{2.5}$ in IGP, however
695   underestimated its magnitude compared to CPCB observations. Moreover, secondary aerosols
696   particularly, chloride aerosols are underestimated in the model. This underestimation is likely caused
697   by a low bias in the residential burning emission inventory and a failure of the emission inventory to
698   represent residential sector emissions from the use of trash as cheap heating fuel properly. AOD
699   regional distribution is predicted well by the model for most of the IGP. However, AOD is
700   underestimated over NWIGP likely due to an underestimation of fugitive emissions during wintertime
701   cold spells.

702   The AR interactions showed a significant impact on meteorology and air quality over IGP. A
703   WRF-chem simulation with AR interactions resulted in a lower PBL height by ~50-270 m compared
704   to a simulation without AR interactions leading to accumulation of aerosols and moisture near the
705   surface. Reduced surface shortwave radiation flux and the surface sensible and latent heat fluxes due
706   to aerosol radiative effect suppressed the turbulence resulting in a stable PBL. The shallow PBL
707   further increased surface PM$_{2.5}$ (> 8 µg m^{-3}) and RH (2-8%) over IGP and this positive feedback
708   mechanism promoted thickening of fog over IGP. However, an increase in absorbing aerosols in the
709   PBL gave negative feedback, increasing the shortwave heating and temperature particularly over
710   CIGP. Fog forms when air is saturated which occurs when the surface temperature is reduced or the
711   moisture content increases causing saturation of air. This study suggests that increase in RH saturated
712   the air and the increase in aerosols favoured fog formation as depicted by the thickening of fog
713   intensity. Aqueous phase chemistry on the other hand contributed significantly to secondary aerosols
714   in the fog, especially sulfate aerosols, indicating substantial formation of secondary aerosols in the
715   cloud. The underpredicted secondary aerosols over NWIGP where no fog occurred implies
716   underestimation of formation of aerosols through gas and aerosol chemistry in the model. This
717   underestimation could also be linked to an underestimation of pH in the default MOSAIC scheme
718   (Ruan et al., 2022) which slows the secondary aerosol formation, or an underestimation of the aqueous
719   sulfur oxidation in haze aerosol at > 80% RH before the onset of fog (Acharja et al., 2022), or missing
720   multiphase oxidation processes (Wang et al., 2022). Nevertheless, we find that the model successfully
721   simulates the same changes in the inorganic composition during fog in IGP as reported by
722   observational studies referred earlier in section 6. We also observed that AR feedback with aqueous
723   chemistry initiated the fog formation 1-2 hours earlier than the initiation time in the simulation
724   without AR feedback and without aqueous phase chemistry whereas AR feedback alone led to early
725   dissipation of fog. In addition, fog acted as an important sink of aerosols in a polluted environment
726   with increased dry deposition with cloud water. Thus, AR feedback and aqueous chemistry play a
727   significant role in modulating the distribution and concentration of aerosols and evolution of fog in the
728   PBL.

729   The large emission of aerosols and trace gases in the IGP makes the atmospheric dynamics as
730   well as chemistry complex, suggesting the need for more studies using both models and ground-based

measurements to better understand the processes. While all aerosol types interact with solar radiation and reduce the surface reaching flux, presence of absorbing aerosols in the boundary layer and its vertical distribution plays an important role in modulating the meteorology over IGP. It is therefore crucial to improve the simulation of absorbing aerosols e.g., BC in the vertical as well as at the surface to increase the accuracy in predicting formation as well as the dissipation of fog in this region. Emissions from burning for residential heating are an important source of aerosols in IGP during post-monsoon and winter and the inclusion of these sources in the emission inventory would improve the prediction of wintertime aerosols. For example, the underestimation of chloride aerosol in the model indicates unaccounted emission sources over IGP and the need for more work on better quantifying trash burning emissions, which may not only improve particulate chloride in the model but also improve simulations of other aerosol chemical components through aerosol thermodynamics. Additionally, more detailed modeling studies are required to understand the missing chemical processes if any in the model which leads to biases in sulfate, nitrate and ammonium partitioning between gas and aerosol phases. We find that the change in PBL height with AR feedback is sensitive to changes in LH, signifying the role of soil moisture in PBL dynamics. Several studies have reported cooling over IGP due to an increase in irrigation (Kumar et al., 2017; Mishra et al., 2020). Further investigations into the role of irrigation in the increasing fog events over NWIGP would help in better understanding the formation and persistence of fog over this region. It can be concluded that fog forecasting is a complex process due to the multiple factors involved and this work suggests that AR feedback is important in fog forecasting while aqueous phase chemistry plays an important role in defining the composition of aerosols over IGP.

Acknowledgement

This material is based upon work supported by the NSF National Center for Atmospheric Research (NCAR), which is a major facility sponsored by the U.S. National Science Foundation under Cooperative Agreement No. 1852977. CB is thankful to the Fulbright Kalam Climate Fellowship program under USIEF (United States – India Educational Foundation), and Women Scientist (WOS-A) program, Department of Science and Technology (DST), Govt of India. The authors acknowledge the use of MODIS data from NASA's Land, Atmosphere Near real-time Capability for EOS (LANCE) system (https://earthdata.nasa.gov/lance), part of NASA's Earth Observing System Data and Information System (EOSDIS); Meteorological & Oceanographic Satellite Data Archival Centre (MOSDAC: https://www.mosdac.gov.in/), Space Applications Centre, Indian Space Research Organisation, Govt. of India for INSAT-3D fog data and the Central Pollution Board of India (CPCB: https://app.cpcbccr.com/ccr/#/login) for meteorology data. We would like to acknowledge the high-performance computing support from Cheyenne (doi:10.5065/D6RX99HX) provided by NCAR's

766 Computational and Information Systems Laboratory. We thank Duseong Jo and Behrooz R, and the
767 two anonymous reviewers for their constructive comments on the manuscript.

768

769 **Data availability:** All the model simulations are archived on the NCAR campaign storage
770 (/glade/campaign/acom/acom-weather/chandrakala) and can be accessed by contacting the
771 corresponding author. WIFEX data can be made available by contacting Dr S.D. Ghude. Trash
772 Burning emission data is available on Mendeley data (doi- http://dx.doi.org/10.17632/t2tn4t9473.1).
773 MODIS AOD retrievals can be downloaded from https://earthdata.nasa. gov/.

774

775 **Author contributions:**
776 CB: Conceptualization, Formal Analysis, Writing
777 MB: Conceptualization, Supervision, Writing-review and editing, Funding acquisition
778 RK: Conceptualization, Supervision, Writing-review and editing
779 SDG: provided ground-based observation data, Writing-review and editing
780 VS and BS: provided trash burning emission data, Writing-review and editing

781

782 **Competing interests:** The authors declare that they have no conflict of interest.

783

784 **References**

785 Acharja, P., Ali, K., Ghude, S. D., Sinha, V., Sinha, B., Kulkarni, R., Gultepe, I. and Rajeevan, M. N.:
786 Enhanced secondary aerosol formation driven by excess ammonia during fog episodes in Delhi, India,
787 Chemosphere, 289(July 2021), 133155, doi:10.1016/j.chemosphere.2021.133155, 2022.

788 Arun, S. H., Sharma, S. K., Chaurasia, S., Vaishnav, R. and Kumar, R.: Fog/low clouds detection over
789 the delhi earth station using the ceilometer and the insat-3d/3dr satellite data, Int. J. Remote Sens.,
790 39(12), 4130–4144, doi:10.1080/01431161.2018.1454624, 2018.

791 Badarinath, K. V. S., Kumar Kharol, S. and Rani Sharma, A.: Long-range transport of aerosols from
792 agriculture crop residue burning in Indo-Gangetic Plains—A study using LIDAR, ground
793 measurements and satellite data, J. Atmos. Solar-Terrestrial Phys., 71(1), 112–120,
794 doi:https://doi.org/10.1016/j.jastp.2008.09.035, 2009.

795 Banerjee, S. and Padmakumari, B.: Spatiotemporal variability and evolution of day and night winter
796 fog over the Indo Gangetic Basin using INSAT-3D and comparison with surface visibility and aerosol
797 optical depth, Sci. Total Environ., 745, 140962, doi:10.1016/j.scitotenv.2020.140962, 2020.

798 Bergot, T. and Guedalia, D.: Numerical Forecasting of Radiation Fog. Part I: Numerical Model and
799 Sensitivity Tests, Mon. Weather Rev., 122(6), 1218–1230, doi:10.1175/1520-
800 0493(1994)122<1218:NFORFP>2.0.CO;2, 1994.

801 Bharali, C., Nair, V. S., Chutia, L. and Babu, S. S.: Modeling of the Effects of Wintertime Aerosols on
802 Boundary Layer Properties Over the Indo Gangetic Plain, J. Geophys. Res. Atmos., 124(7), 4141–
803 4157, doi:10.1029/2018JD029758, 2019.

804 Bodaballa, J. K., Geresdi, I., Ghude, S. D. and Salma, I.: Numerical simulation of the microphysics
805 and liquid chemical processes occur in fog using size resolving bin scheme, Atmos. Res., 266,
806 105972, doi:https://doi.org/10.1016/j.atmosres.2021.105972, 2022.

807 Boutle, I., Price, J., Kudzotsa, I., Kokkola, H. and Romakkaniemi, S.: Aerosol-fog interaction and the
808 transition to well-mixed radiation fog, Atmos. Chem. Phys., 18(11), 7827–7840, doi:10.5194/acp-18-
809 7827-2018, 2018.

810 Bran, S. H. and Srivastava, R.: Investigation of PM(2.5) mass concentration over India using a
811 regional climate model., Environ. Pollut., 224, 484–493, doi:10.1016/j.envpol.2017.02.030, 2017.

812 Chapman, E. G., Gustafson, W. I., Easter, R. C., Barnard, J. C., Ghan, S. J., Pekour, M. S. and Fast, J.
813 D.: Coupling aerosol-cloud-radiative processes in the WRF-Chem model: Investigating the radiative
814 impact of elevated point sources, Atmos. Chem. Phys., 9(3), 945–964, doi:10.5194/acp-9-945-2009,
815 2009.

816 Chaudhary, P., Garg, S., George, T., Shabin, M., Saha, S., Subodh, S. and Sinha, B.: Underreporting
817 and open burning – the two largest challenges for sustainable waste management in India, Resour.
818 Conserv. Recycl., 175(July), 105865, doi:10.1016/j.resconrec.2021.105865, 2021.

819 Chaurasia, S. and Gohil, B. S.: Detection of Day Time Fog over India Using INSAT-3D Data, IEEE J.
820 Sel. Top. Appl. Earth Obs. Remote Sens., 8(9), 4524–4530, doi:10.1109/JSTARS.2015.2493000,
821 2015.

822 Chaurasia, S. and Jenamani, R. K.: Detection of Fog Using Temporally Consistent, , 10(12), 5307–
823 5313, 2017.

824 Chen, C., Zhang, M., Perrie, W., Chang, R., Chen, X., Duplessis, P. and Wheeler, M.: Boundary Layer
825 Parameterizations to Simulate Fog Over Atlantic Canada Waters, Earth Sp. Sci., 7(3),
826 doi:10.1029/2019EA000703, 2020.

827 David, L. M., Ravishankara, A. R., Kodros, J. K., Venkataraman, C., Sadavarte, P., Pierce, J. R.,
828 Chaliyakunnel, S. and Millet, D. B.: Aerosol Optical Depth Over India, J. Geophys. Res. Atmos.,
829 123(7), 3688–3703, doi:10.1002/2017JD027719, 2018.

830 Debnath, S., Karumuri, R. K., Govardhan, G., Jat, R., Saini, H., Vispute, A., Kulkarni, S. H., Jena, C.,
831 Kumar, R., Chate, D. M. and Ghude, S. D.: Implications of Implementing Promulgated and
832 Prospective Emission Regulations on Air Quality and Health in India during 2030 N3   -
833 10.4209/aaqr.220112,   AEROSOL   AIR   Qual.   Res.   [online]   Available   from:

834 http://hdl.handle.net/10754/681704, 2022.

835 Deshpande, P., Meena, D., Tripathi, S., Bhattacharya, A. and Verma, M. K.: Event-based fog

836 climatology and typology for cities in Indo-Gangetic plains, Urban Clim., 51, 101642,

837 doi:https://doi.org/10.1016/j.uclim.2023.101642, 2023.

838 Dey, S. and Di Girolamo, L.: A decade of change in aerosol properties over the Indian subcontinent,

839 Geophys. Res. Lett., 38(14), 1–5, doi:10.1029/2011GL048153, 2011.

840 Dey, S. and Tripathi, S. N.: Estimation of aerosol optical properties and radiative effects in the Ganga

841 basin, northern India, during the wintertime, J. Geophys. Res. Atmos., 112(3),

842 doi:10.1029/2006JD007267, 2007.

843 Dhangar, N. G., Lal, D. M., Ghude, S. D., Kulkarni, R., Parde, A. N., Pithani, P., Niranjan, K., Prasad,

844 D. S. V. V. D., Jena, C., Sajjan, V. S., Prabhakaran, T., Karipot, A. K., Jenamani, R. K., Singh, S. and

845 Rajeevan, M.: On the Conditions for Onset and Development of Fog Over New Delhi: An

846 Observational Study from the WiFEX, Pure Appl. Geophys., 178(9), 3727–3746, doi:10.1007/s00024-

847 021-02800-4, 2021.

848 Ding, A. J., Huang, X., Nie, W., Sun, J. N., Kerminen, V. M., Petäjä, T., Su, H., Cheng, Y. F., Yang,

849 X. Q., Wang, M. H., Chi, X. G., Wang, J. P., Virkkula, A., Guo, W. D., Yuan, J., Wang, S. Y., Zhang,

850 R. J., Wu, Y. F., Song, Y., Zhu, T., Zilitinkevich, S., Kulmala, M. and Fu, C. B.: Enhanced haze

851 pollution by black carbon in megacities in China, Geophys. Res. Lett., 43(6), 2873–2879,

852 doi:10.1002/2016GL067745, 2016.

853 Easter, R. C., Ghan, S. J., Zhang, Y., Saylor, R. D., Chapman, E. G., Laulainen, N. S., Abdul-Razzak,

854 H., Leung, L. R., Bian, X. and Zaveri, R. A.: MIRAGE: Model description and evaluation of aerosols

855 and trace gases, J. Geophys. Res. D Atmos., 109(20), doi:10.1029/2004JD004571, 2004.

856 Emmons, L. K., Schwantes, R. H., Orlando, J. J., Tyndall, G., Kinnison, D., Lamarque, J. F., Marsh,

857 D., Mills, M. J., Tilmes, S., Bardeen, C., Buchholz, R. R., Conley, A., Gettelman, A., Garcia, R.,

858 Simpson, I., Blake, D. R., Meinardi, S. and Pétron, G.: The Chemistry Mechanism in the Community

859 Earth System Model Version 2 (CESM2), J. Adv. Model. Earth Syst., 12(4), 1–21,

860 doi:10.1029/2019MS001882, 2020.

861 Emmons, L. K., Walters, S., Hess, P. G., Lamarque, J. F., Pfister, G. G., Fillmore, D., Granier, C.,

862 Guenther, A., Kinnison, D., Laepple, T., Orlando, J., Tie, X., Tyndall, G., Wiedinmyer, C.,

863 Baughcum, S. L. and Kloster, S.: Description and evaluation of the Model for Ozone and Related

864 chemical Tracers, version 4 (MOZART-4), Geosci. Model Dev., 3(1), 43–67, doi:10.5194/gmd-3-43-

865 2010, 2010.

866 Fahey, K. M. and Pandis, S. N.: Optimizing model performance: variable size resolution in cloud

867 chemistry modeling, Atmos. Environ., 35(26), 4471–4478, doi:https://doi.org/10.1016/S1352-

868 2310(01)00224-2, 2001.

869 Fast, J. D., Gustafson Jr, W. I., Easter, R. C., Zaveri, R. A., Barnard, J. C., Chapman, E. G., Grell, G.
870 A. and Peckham, S. E.: Evolution of ozone, particulates, and aerosol direct forcing in an urban area
871 using a new fully-coupled meteorology, chemistry, and aerosol model, J. Geophys. Res, 111(5),
872 D21305, 2006.

873 Gautam, R., Hsu, N. C., Kafatos, M. and Tsay, S.: Influences of winter haze on fog / low cloud over
874 the Indo-Gangetic plains, , 112(June 2006), 1–11, doi:10.1029/2005JD007036, 2007.

875 Ghude, S. D., Bhat, G. S., Prabhakaran, T., Jenamani, R. K., Chate, D. M., Safai, P. D., Karipot, A.
876 K., Konwar, M., Pithani, P., Sinha, V., Rao, P. S. P., Dixit, S. A., Tiwari, S., Todekar, K., Varpe, S.,
877 Srivastava, A. K., Bisht, D. S., Murugavel, P., Ali, K., Mina, U., Dharua, M., Jaya Rao, Y.,
878 Padmakumari, B., Hazra, A., Nigam, N., Shende, U., Lal, D. M., Chandra, B. P., Mishra, A. K.,
879 Kumar, A., Hakkim, H., Pawar, H., Acharja, P., Kulkarni, R., Subharthi, C., Balaji, B., Varghese, M.,
880 Bera, S. and Rajeevan, M.: Winter fog experiment over the Indo-Gangetic plains of India, Curr. Sci.,
881 112(4), 767–784, doi:10.18520/cs/v112/i04/767-784, 2017.

882 Ghude, S. D., Chate, D. M., Jena, C., Beig, G., Kumar, R., Barth, M. C., Pfister, G. G., Fadnavis, S.
883 and Pithani, P.: Premature mortality in India due to PM2.5 and ozone exposure, Geophys. Res. Lett.,
884 43(9), 4650–4658, doi:https://doi.org/10.1002/2016GL068949, 2016.

885 Ghude, S. D., Jenamani, R. K., Kulkarni, R., Wagh, S., Dhangar, N. G., Parde, A. N., Acharja, P.,
886 Lonkar, P., Govardhan, G., Yadav, P., Vispute, A., Debnath, S., Lal, D. M., Bisht, D. S., Jena, C.,
887 Pawar, P. V., Dhankhar, S. S., Sinha, V., Chate, D. M., Safai, P. D., Nigam, N., Konwar, M., Hazra,
888 A., Dharmaraj, T., Gopalkrishnan, V., Padmakumari, B., Gultepe, I., Biswas, M., Karipot, A. K.,
889 Prabhakaran, T., Nanjundiah, R. S. and Rajeevan, M.: WiFEX Walk into the Warm Fog over Indo-
890 Gangetic Plain Region, Bull. Am. Meteorol. Soc., 104(5), E980–E1005, doi:10.1175/BAMS-D-21-
891 0197.1, 2023.

892 Ghude, S. D., Kulkarni, S. H., Jena, C., Pfister, G. G., Beig, G., Fadnavis, S. and Van Der, R. J.:
893 Application of satellite observations for identifying regions of dominant sources of nitrogen oxides
894 over the indian subcontinent, J. Geophys. Res. Atmos., 118(2), 1075–1089,
895 doi:10.1029/2012JD017811, 2013.

896 Ghude, S. D., Kumar, R., Jena, C., Debnath, S., Kulkarni, R. G., Alessandrini, S., Biswas, M.,
897 Kulkrani, S., Pithani, P., Kelkar, S., Sajjan, V., Chate, D. M., Soni, V. K., Singh, S., Nanjundiah, R. S.
898 and Rajeevan, M.: Evaluation of PM2.5 forecast using chemical data assimilation in the WRF-Chem
899 model: A novel initiative under the Ministry of Earth Sciences Air Quality Early Warning System for
900 Delhi, India, Curr. Sci., 118(11), 1803–1815, doi:10.18520/cs/v118/i11/1803-1815, 2020.

901 Govardhan, G., Nanjundiah, R. S., Satheesh, S. K., Krishnamoorthy, K. and Kotamarthi, V. R.:

Performance of WRF-chem over indian region: Comparison with measurements, J. Earth Syst. Sci., 124(4), 875–896, doi:10.1007/s12040-015-0576-7, 2015.

Grell, G. A., Peckham, S. E., Schmitz, R., McKeen, S. A., Frost, G., Skamarock, W. C. and Eder, B.: Fully coupled "online" chemistry within the WRF model, Atmos. Environ., 39(37), 6957–6975, doi:https://doi.org/10.1016/j.atmosenv.2005.04.027, 2005.

Guenther, A., Karl, T., Harley, P., Weidinmyer, C., Palmer, P. I. and Geron, C.: Edinburgh Research Explorer Estimates of global terrestrial isoprene emissions using MEGAN (Model of Emissions of Gases and Aerosols from Nature) and Physics Estimates of global terrestrial isoprene emissions using MEGAN (Model of Emissions of Gases an, Atmos. Chem. Phys., (6), 3181–3210, 2006.

Gundel, L. A., Benner, W. H. and Hansen, A. D. A.: Chemical composition of fog water and interstitial aerosol in Berkeley, California, Atmos. Environ., 28(16), 2715–2725, doi:https://doi.org/10.1016/1352-2310(94)90443-X, 1994.

Gupta, T. and Mandariya, A.: Sources of submicron aerosol during fog-dominated wintertime at Kanpur, Environ. Sci. Pollut. Res., 20(8), 5615–5629, doi:10.1007/s11356-013-1580-6, 2013.

Hakkim, H., Sinha, V., Chandra, B. P., Kumar, A., Mishra, A. K., Sinha, B., Sharma, G., Pawar, H., Sohpaul, B., Ghude, S. D., Pithani, P., Kulkarni, R., Jenamani, R. K. and Rajeevan, M.: Volatile organic compound measurements point to fog-induced biomass burning feedback to air quality in the megacity of Delhi, Sci. Total Environ., 689, 295–304, doi:10.1016/j.scitotenv.2019.06.438, 2019.

Hong, S. Y., Noh, Y. and Dudhia, J.: A new vertical diffusion package with an explicit treatment of entrainment processes, Mon. Weather Rev., 134(9), 2318–2341, doi:10.1175/MWR3199.1, 2006.

Jacobson, M. Z., Turco, R. P., Jensen, E. J. and Toon, O. B.: Modeling coagulation among particles of different composition and size, Atmos. Environ., 28(7), 1327–1338, doi:https://doi.org/10.1016/1352-2310(94)90280-1, 1994.

Jain, S., Sharma, S. K., Vijayan, N. and Mandal, T. K.: Seasonal characteristics of aerosols (PM2.5 and PM10) and their source apportionment using PMF: A four year study over Delhi, India, Elsevier Ltd., 2020.

Jena, C., Ghude, S. D., Kumar, R., Debnath, S., Govardhan, G., Soni, V. K., Kulkarni, S. H., Beig, G., Nanjundiah, R. S. and Rajeevan, M.: Performance of high resolution (400 m) PM2.5 forecast over Delhi, Sci. Rep., 11(1), 1–9, doi:10.1038/s41598-021-83467-8, 2021.

Jena, C., Ghude, S., Kulkarni, R., Debnath, S., Kumar, R., Soni, V. K., Acharja, P., Kulkarni, S., Khare, M., Kaginalkar, A., Chate, D., Ali, K., Nanjundiah, R. and Rajeevan, M.: Evaluating the sensitivity of fine particulate matter (PM$_{2.5}$) simulations to chemical mechanism in Delhi, Atmos. Chem. Phys. Discuss., (3), 1–28, 2020.

935 Jenamani, R. K.: Alarming rise in fog and pollution causing a fall in maximum temperature over
936 Delhi, Curr. Sci., 93(3), 314–322 [online] Available from: http://www.jstor.org/stable/24099461,
937 2007.

938 Jethva, H., Chand, D., Torres, O., Gupta, P., Lyapustin, A. and Patadia, F.: Agricultural burning and
939 air quality over northern india: A synergistic analysis using nasa's a-train satellite data and ground
940 measurements, Aerosol Air Qual. Res., 18(7), 1756–1773, doi:10.4209/aaqr.2017.12.0583, 2018.

941 Katata, G., Chino, M., Kobayashi, T., Terada, H., Ota, M., Nagai, H., Kajino, M., Draxler, R., Hort,
942 M. C., Malo, A., Torii, T. and Sanada, Y.: Detailed source term estimation of the atmospheric release
943 for the Fukushima Daiichi Nuclear Power Station accident by coupling simulations of an atmospheric
944 dispersion model with an improved deposition scheme and oceanic dispersion model, Atmos. Chem.
945 Phys., 15(2), 1029–1070, doi:10.5194/acp-15-1029-2015, 2015.

946 Kaul, D. S., Gupta, T., Tripathi, S. N., Tare, V. and Collett, J. L.: Secondary organic aerosol: A
947 comparison between foggy and nonfoggy days, Environ. Sci. Technol., 45(17), 7307–7313,
948 doi:10.1021/es201081d, 2011.

949 Kedia, S., Ramachandran, S., Holben, B. N. and Tripathi, S. N.: Quantification of aerosol type, and
950 sources of aerosols over the Indo-Gangetic Plain, Atmos. Environ., 98, 607–619,
951 doi:10.1016/j.atmosenv.2014.09.022, 2014.

952 Knote, C., Tuccella, P., Curci, G., Emmons, L., Orlando, J. J., Madronich, S., Baró, R., Jiménez-
953 Guerrero, P., Luecken, D., Hogrefe, C., Forkel, R., Werhahn, J., Hirtl, M., Pérez, J. L., San José, R.,
954 Giordano, L., Brunner, D., Yahya, K. and Zhang, Y.: Influence of the choice of gas-phase mechanism
955 on predictions of key gaseous pollutants during the AQMEII phase-2 intercomparison, Atmos.
956 Environ., 115, 553–568, doi:10.1016/j.atmosenv.2014.11.066, 2014.

957 Krishna Moorthy, K., Suresh Babu, S., Manoj, M. R. and Satheesh, S. K.: Buildup of aerosols over the
958 Indian Region, Geophys. Res. Lett., 40(5), 1011–1014, doi:10.1002/grl.50165, 2013.

959 Krishna, R. K., Panicker, A. S., Yusuf, A. M. and Ullah, B. G.: On the contribution of particulate
960 matter (PM 2.5) to direct radiative forcing over two urban environments in India, Aerosol Air Qual.
961 Res., 19(2), 399–410, doi:10.4209/aaqr.2018.04.0128, 2019.

962 Kulkarni, R., Jenamani, R. K., Pithani, P. and Konwar, M.: Loss to Aviation Economy Due to Winter
963 Fog in New Delhi during the Winter of 2011 – 2016, , 1–10, 2019.

964 Kulkarni, S. H., Ghude, S. D., Jena, C., Karumuri, R. K., Sinha, B., Sinha, V., Kumar, R., Soni, V. K.
965 and Khare, M.: How Much Does Large-Scale Crop Residue Burning Affect the Air Quality in Delhi?,
966 Environ. Sci. Technol., 54(8), 4790–4799, doi:10.1021/acs.est.0c00329, 2020.

967 Kumar, A. and Sarin, M. M.: Aerosol iron solubility in a semi-arid region: temporal trend and impact

968   of anthropogenic sources, Tellus B, 62(2), doi:10.3402/tellusb.v62i2.16519, 2010.

969   Kumar, A., Hakkim, H., Sinha, B. and Sinha, V.: Gridded 1 km × 1 km emission inventory for paddy
970   stubble burning emissions over north-west India constrained by measured emission factors of 77
971   VOCs and district-wise crop yield data, Sci. Total Environ., 789, 148064,
972   doi:10.1016/j.scitotenv.2021.148064, 2021.

973   Kumar, M., Parmar, K. S., Kumar, D. B., Mhawish, A., Broday, D. M., Mall, R. K. and Banerjee, T.:
974   Long-term aerosol climatology over Indo-Gangetic Plain: Trend, prediction and potential source
975   fields, Atmos. Environ., 180, 37–50, doi:10.1016/j.atmosenv.2018.02.027, 2018.

976   Kumar, R., Barth, M. C., Pfister, G. G., Nair, V. S., Ghude, S. D. and Ojha, N.: What controls the
977   seasonal cycle of black carbon aerosols in India?, J. Geophys. Res. Atmos., 120(15), 7788–7812,
978   doi:https://doi.org/10.1002/2015JD023298, 2015.

979   Kumar, R., Ghude, S. D., Biswas, M., Jena, C., Alessandrini, S., Debnath, S., Kulkarni, S., Sperati, S.,
980   Soni, V. K., Nanjundiah, R. S. and Rajeevan, M.: Enhancing Accuracy of Air Quality and
981   Temperature Forecasts During Paddy Crop Residue Burning Season in Delhi Via Chemical Data
982   Assimilation., 2020.

983   Kumar, R., Mishra, V., Buzan, J., Kumar, R., Shindell, D. and Huber, M.: Dominant control of
984   agriculture and irrigation on urban heat island in India, Sci. Rep., 7(1), 1–11, doi:10.1038/s41598-017-
985   14213-2, 2017.

986   Lalchandani, V., Kumar, V., Tobler, A., M. Thamban, N., Mishra, S., Slowik, J. G., Bhattu, D., Rai,
987   P., Satish, R., Ganguly, D., Tiwari, S., Rastogi, N., Tiwari, S., Močnik, G., Prévôt, A. S. H. and
988   Tripathi, S. N.: Real-time characterization and source apportionment of fine particulate matter in the
989   Delhi megacity area during late winter, Sci. Total Environ., 770, doi:10.1016/j.scitotenv.2021.145324,
990   2021.

991   Lelieveld, J., Evans, J. S., Fnais, M., Giannadaki, D. and Pozzer, A.: The contribution of outdoor air
992   pollution sources to premature mortality on a global scale, Nature, 525(7569), 367–371,
993   doi:10.1038/nature15371, 2015.

994   Ma, Y., Brooks, S. D., Vidaurre, G., Khalizov, A. F., Wang, L. and Zhang, R.: Rapid modification of
995   cloud-nucleating ability of aerosols by biogenic emissions, Geophys. Res. Lett., 40(23), 6293–6297,
996   doi:https://doi.org/10.1002/2013GL057895, 2013.

997   Maalick, Z., Kühn, T., Korhonen, H., Kokkola, H., Laaksonen, A. and Romakkaniemi, S.: Effect of
998   aerosol concentration and absorbing aerosol on the radiation fog life cycle, Atmos. Environ., 133, 26–
999   33, doi:10.1016/j.atmosenv.2016.03.018, 2016.

1000   Mandariya, A. K., Gupta, T. and Tripathi, S. N.: Effect of aqueous-phase processing on the formation

and evolution of organic aerosol (OA) under different stages of fog life cycles, Atmos. Environ., 206(November 2018), 60–71, doi:10.1016/j.atmosenv.2019.02.047, 2019.

Martin, L. R. and Good, T. W.: Catalyzed oxidation of sulfur dioxide in solution: The iron-manganese synergism, Atmos. Environ. Part A, Gen. Top., 25(10), 2395–2399, doi:10.1016/0960-1686(91)90113-L, 1991.

Mishra, V., Ambika, A. K., Asoka, A., Aadhar, S., Buzan, J., Kumar, R. and Huber, M.: Moist heat stress extremes in India enhanced by irrigation, Nat. Geosci., 13(11), 722–728, doi:10.1038/s41561-020-00650-8, 2020.

Mohan, M. and Gupta, M.: Sensitivity of PBL parameterizations on PM10 and ozone simulation using chemical transport model WRF-Chem over a sub-tropical urban airshed in India, Atmos. Environ., 185, 53–63, doi:10.1016/j.atmosenv.2018.04.054, 2018.

Moore, R. H., Cerully, K., Bahreini, R., Brock, C. A., Middlebrook, A. M. and Nenes, A.: Hygroscopicity and composition of California CCN during summer 2010, J. Geophys. Res. Atmos., 117(7), 1–14, doi:10.1029/2011JD017352, 2012.

Nagpure, A. S., Ramaswami, A. and Russell, A.: Characterizing the Spatial and Temporal Patterns of Open Burning of Municipal Solid Waste (MSW) in Indian Cities, Environ. Sci. Technol., 49(21), 12904–12912, doi:10.1021/acs.est.5b03243, 2015.

Neu, J. L. and Prather, M. J.: Toward a more physical representation of precipitation scavenging in global chemistry models: Cloud overlap and ice physics and their impact on tropospheric ozone, Atmos. Chem. Phys., 12(7), 3289–3310, doi:10.5194/acp-12-3289-2012, 2012.

Ojha, N., Sharma, A., Kumar, M., Girach, I., Ansari, T. U., Sharma, S. K., Singh, N., Pozzer, A. and Gunthe, S. S.: On the widespread enhancement in fine particulate matter across the Indo-Gangetic Plain towards winter, Sci. Rep., 10(1), 1–9, doi:10.1038/s41598-020-62710-8, 2020.

Pan, X., Chin, M., Gautam, R., Bian, H., Kim, D., Colarco, P. R., Diehl, T. L., Takemura, T., Pozzoli, L., Tsigaridis, K., Bauer, S. and Bellouin, N.: A multi-model evaluation of aerosols over South Asia: Common problems and possible causes, Atmos. Chem. Phys., 15(10), 5903–5928, doi:10.5194/acp-15-5903-2015, 2015.

Pant, P., Shukla, A., Kohl, S. D., Chow, J. C., Watson, J. G. and Harrison, R. M.: Characterization of ambient PM2.5 at a pollution hotspot in New Delhi, India and inference of sources, Atmos. Environ., 109, 178–189, doi:10.1016/j.atmosenv.2015.02.074, 2015.

Patil, R. S., Kumar, R., Menon, R., Shah, M. K. and Sethi, V.: Development of particulate matter speciation profiles for major sources in six cities in India, Atmos. Res., 132–133, 1–11, doi:10.1016/j.atmosres.2013.04.012, 2013.

1034 Pawar, H. and Sinha, B.: Residential heating emissions (can) exceed paddy-residue burning emissions

1035 in rural northwest India, Atmos. Environ., 269, 118846,

1036 doi:https://doi.org/10.1016/j.atmosenv.2021.118846, 2022.

1037 Pawar, P. V., Ghude, S. D., Govardhan, G., Acharja, P., Kulkarni, R., Kumar, R., Sinha, B., Sinha, V.,

1038 Jena, C., Gunwani, P., Adhya, T. K., Nemitz, E. and Sutton, M. A.: Chloride (HCl / Cl-) dominates

1039 inorganic aerosol formation from ammonia in the Indo-Gangetic Plain during winter: modeling and

1040 comparison with observations, Atmos. Chem. Phys., 23(1), 41–59, doi:10.5194/acp-23-41-2023, 2023.

1041 Pithani, P., Ghude, S. D., Chennu, V. N., Kulkarni, R. G., Steeneveld, G. J., Sharma, A., Prabhakaran,

1042 T., Chate, D. M., Gultepe, I, Jenamani, R. K. and Madhavan, R.: WRF Model Prediction of a Dense

1043 Fog Event Occurred During the Winter Fog Experiment (WIFEX), Pure Appl. Geophys., 176(4),

1044 1827–1846, doi:10.1007/s00024-018-2053-0, 2019.

1045 Pithani, P., Ghude, S. D., Jenamani, R. K., Biswas, M., Naidu, C. V., Debnath, S., Kulkarni, R.,

1046 Dhangar, N. G., Jena, C., Hazra, A., Phani, R., Mukhopadhyay, P., Prabhakaran, T., Nanjundiah, R. S.

1047 and Rajeevan, M.: Real-time forecast of dense fog events over Delhi: The performance of the wrf

1048 model during the wifex field campaign, Weather Forecast., 35(2), 739–756, doi:10.1175/WAF-D-19-

1049 0104.1, 2020.

1050 Pleim, J. E. and Chang, J. S.: A non-local closure model for vertical mixing in the convective

1051 boundary layer, Atmos. Environ. Part A. Gen. Top., 26(6), 965–981, doi:https://doi.org/10.1016/0960-

1052 1686(92)90028-J, 1992.

1053 Pleim, J. E. and Gilliam, R.: An indirect data assimilation scheme for deep soil temperature in the

1054 Pleim-Xiu land surface model, J. Appl. Meteorol. Climatol., 48(7), 1362–1376,

1055 doi:10.1175/2009JAMC2053.1, 2009.

1056 Pleim, J. E. and Xiu, A.: Development of a land surface model. Part II: Data assimilation, J. Appl.

1057 Meteorol., 42(12), 1811–1822, doi:10.1175/1520-0450(2003)042<1811:DOALSM>2.0.CO;2, 2003.

1058 Pleim, J. E.: A combined local and nonlocal closure model for the atmospheric boundary layer. Part I:

1059 Model description and testing, J. Appl. Meteorol. Climatol., 46(9), 1383–1395,

1060 doi:10.1175/JAM2539.1, 2007a.

1061 Pleim, J. E.: A combined local and nonlocal closure model for the atmospheric boundary layer. Part II:

1062 Application and evaluation in a mesoscale meteorological model, J. Appl. Meteorol. Climatol., 46(9),

1063 1396–1409, doi:10.1175/JAM2534.1, 2007b.

1064 Powers, J. G., Klemp, J. B., Skamarock, W. C., Davis, C. A., Dudhia, J., Gill, D. O., Coen, J. L.,

1065 Gochis, D. J., Ahmadov, R., Peckham, S. E., Grell, G. A., Michalakes, J., Trahan, S., Benjamin, S. G.,

1066 Alexander, C. R., Dimego, G. J., Wang, W., Schwartz, C. S., Romine, G. S., Liu, Z., Snyder, C.,

1067 Chen, F., Barlage, M. J., Yu, W. and Duda, M. G.: The weather research and forecasting model:

1068 Overview, system efforts, and future directions, Bull. Am. Meteorol. Soc., 98(8), 1717–1737,
1069 doi:10.1175/BAMS-D-15-00308.1, 2017.

1070 Pye, H. O. T., Nenes, A., Alexander, B., Ault, A. P., Barth, M. C., Clegg, S. L., Collett, J. L., Fahey,
1071 K. M., Hennigan, C. J., Herrmann, H., Kanakidou, M., Kelly, J. T., Ku, I. T., Faye McNeill, V.,
1072 Riemer, N., Schaefer, T., Shi, G., Tilgner, A., Walker, J. T., Wang, T., Weber, R., Xing, J., Zaveri, R.
1073 A. and Zuend, A.: The acidity of atmospheric particles and clouds., 2020.

1074 Ram, K., Sarin, M. M. and Tripathi, S. N.: Temporal trends in atmospheric PM 2.5, PM 10, elemental
1075 carbon, organic carbon, water-soluble organic carbon, and optical properties: Impact of biomass
1076 burning emissions in the Indo-Gangetic Plain, Environ. Sci. Technol., 46(2), 686–695,
1077 doi:10.1021/es202857w, 2012b.

1078 Ram, K., Sarin, M. M., Sudheer, A. K. and Rengarajan, R.: Carbonaceous and secondary inorganic
1079 aerosols during wintertime fog and haze over urban sites in the Indo-Gangetic plain, Aerosol Air Qual.
1080 Res., 12(3), 355–366, doi:10.4209/aaqr.2011.07.0105, 2012a.

1081 Ramachandran, S., Rupakheti, M. and Lawrence, M. G.: Aerosol-induced atmospheric heating rate
1082 decreases over South and East Asia as a result of changing content and composition, Sci. Rep., 10(1),
1083 1–17, doi:10.1038/s41598-020-76936-z, 2020.

1084 Rengarajan, R., Sarin, M. M. and Sudheer, A. K.: Carbonaceous and inorganic species in atmospheric
1085 aerosols during wintertime over urban and high-altitude sites in North India, J. Geophys. Res. Atmos.,
1086 112(21), 1–16, doi:10.1029/2006JD008150, 2007.

1087 Ruan, X., Zhao, C., Zaveri, R. A., He, P., Wang, X., Shao, J. and Geng, L.: Simulations of aerosol pH
1088 in China using WRF-Chem (v4 . 0): sensitivities of aerosol pH and its temporal variations during
1089 haze episodes, , 6143–6164, 2022.

1090 Safai, P. D., Ghude, S., Pithani, P., Varpe, S., Kulkarni, R., Todekar, K., Tiwari, S., Chate, D. M.,
1091 Prabhakaran, T., Jenamani, R. K. and Rajeevan, M. N.: Two-way relationship between aerosols and
1092 fog: A case study at IGI airport, New Delhi, Aerosol Air Qual. Res., 19(1), 71–79,
1093 doi:10.4209/aaqr.2017.11.0542, 2019.

1094 Sarkar, C., Roy, A., Chatterjee, A., Ghosh, S. K. and Raha, S.: Factors controlling the long-term
1095 (2009–2015) trend of PM2.5 and black carbon aerosols at eastern Himalaya, India, Sci. Total
1096 Environ., 656, 280–296, doi:10.1016/j.scitotenv.2018.11.367, 2019.

1097 Sarkar, S., Chokngamwong, R., Cervone, G., Singh, R. P. and Kafatos, M.: Variability of aerosol
1098 optical depth and aerosol forcing over India, Adv. Sp. Res., 37(12), 2153–2159,
1099 doi:10.1016/j.asr.2005.09.043, 2006.

1100 Sengupta, A., Govardhan, G., Debnath, S., Yadav, P., Kulkarni, S. H., Parde, A. N., Lonkar, P.,

1101 Dhangar, N., Gunwani, P., Wagh, S., Nivdange, S., Jena, C., Kumar, R. and Ghude, S. D.: Probing
1102 into the wintertime meteorology and particulate matter (PM2.5 and PM10) forecast over Delhi,
1103 Atmos. Pollut. Res., 13(6), 101426, doi:https://doi.org/10.1016/j.apr.2022.101426, 2022.

1104 Shao, N., Lu, C., Jia, X., Wang, Y., Li, Y., Yin, Y., Zhu, B., Zhao, T., Liu, D., Niu, S., Fan, S., Yan,
1105 S. and Lv, J.: Self-enhanced aerosol – fog interactions in two successive radiation fog events in the
1106 Yangtze River Delta , China : A simulation study, , (January), 1–46, 2023.

1107 Sharma, A. R., Kharol, S. K., Badarinath, K. V. S. and Singh, D.: Impact of agriculture crop residue
1108 burning on atmospheric aerosol loading - A study over Punjab State, India, Ann. Geophys., 28(2),
1109 367–379, doi:10.5194/angeo-28-367-2010, 2010.

1110 Sharma, G., Annadate, S. and Sinha, B.: Will open waste burning become India ' s largest air
1111 pollution source ? ☆, Environ. Pollut., 292(PA), 118310, doi:10.1016/j.envpol.2021.118310, 2022.

1112 Sharma, S. K. and Mandal, T. K.: Elemental Composition and Sources of Fine Particulate Matter
1113 (PM2.5) in Delhi, India, Bull. Environ. Contam. Toxicol., 110(3), 1–8, doi:10.1007/s00128-023-
1114 03707-7, 2023.

1115 Singh, A. and Dey, S.: Influence of aerosol composition on visibility in megacity Delhi, Atmos.
1116 Environ., 62, 367–373, doi:10.1016/j.atmosenv.2012.08.048, 2012.

1117 Singh, N., Banerjee, T., Raju, M. P., Deboudt, K., Sorek-Hamer, M., Singh, R. S. and Mall, R. K.:
1118 Aerosol chemistry, transport, and climatic implications during extreme biomass burning emissions
1119 over the Indo-Gangetic Plain, Atmos. Chem. Phys., 18(19), 14197–14215, doi:10.5194/acp-18-14197-
1120 2018, 2018.

1121 Srinivas, B. and Sarin, M. M.: PM2.5, EC and OC in atmospheric outflow from the Indo-Gangetic
1122 Plain: Temporal variability and aerosol organic carbon-to-organic mass conversion factor, Sci. Total
1123 Environ., 487(1), 196–205, doi:10.1016/j.scitotenv.2014.04.002, 2014.

1124 Srivastava, P., Dey, S., Srivastava, A. K., Singh, S. and Tiwari, S.: Most probable mixing state of
1125 aerosols in Delhi NCR, northern India, Atmos. Res., 200(September 2017), 88–96,
1126 doi:10.1016/j.atmosres.2017.09.018, 2018.

1127 Steeneveld, G. J., Ronda, R. J. and Holtslag, A. A. M.: The Challenge of Forecasting the Onset and
1128 Development of Radiation Fog Using Mesoscale Atmospheric Models, Boundary-Layer Meteorol.,
1129 154(2), 265–289, doi:10.1007/s10546-014-9973-8, 2015.

1130 Stolaki, S., Haeffelin, M., Lac, C., Dupont, J. C., Elias, T. and Masson, V.: Influence of aerosols on
1131 the life cycle of a radiation fog event. A numerical and observational study, Atmos. Res., 151, 146–
1132 161, doi:10.1016/j.atmosres.2014.04.013, 2015.

1133 Syed, F. S., Körnich, H. and Tjernström, M.: On the fog variability over south Asia, Clim. Dyn.,

39(12), 2993–3005, doi:10.1007/s00382-012-1414-0, 2012.

Tare, V., Tripathi, S. N., Chinnam, N., Srivastava, A. K., Dey, S., Manar, M., Kanawade, V. P., Agarwal, A., Kishore, S., Lal, R. B. and Sharma, M.: Measurements of atmospheric parameters during Indian Space Research Organization Geosphere Biosphere Program Land Campaign II at a typical location in the Ganga basin: 2. Chemical properties, J. Geophys. Res. Atmos., 111(23), doi:10.1029/2006JD007279, 2006.

Tav, J., Masson, O., Burnet, F., Paulat, P., Bourrianne, T., Conil, S. and Pourcelot, L.: Determination of fog-droplet deposition velocity from a simple weighing method, Aerosol Air Qual. Res., 18(1), 103–113, doi:10.4209/aaqr.2016.11.0519, 2018.

Taylor, K. E.: in a Single Diagram, , 106, 7183–7192, 2001.

Van Der Velde, I. R., Steeneveld, G. J., Wichers Schreur, B. G. J. and Holtslag, A. A. M.: Modeling and forecasting the onset and duration of severe radiation fog under frost conditions, Mon. Weather Rev., 138(11), 4237–4253, doi:10.1175/2010MWR3427.1, 2010.

Verma, S., Ramana, M. V. and Kumar, R.: Atmospheric rivers fueling the intensification of fog and haze over Indo-Gangetic Plains, Sci. Rep., 12(1), 1–9, doi:10.1038/s41598-022-09206-9, 2022.

Wang, T., Liu, M., Liu, M., Song, Y., Xu, Z., Shang, F., Huang, X., Liao, W., Wang, W., Ge, M., Cao, J., Hu, J., Tang, G., Pan, Y., Hu, M. and Zhu, T.: Sulfate Formation Apportionment during Winter Haze Events in North China, Environ. Sci. Technol., 56(12), 7771–7778, doi:10.1021/acs.est.2c02533, 2022.

Wexler, A. S., Lurmann, F. W. and Seinfeld, J. H.: Modelling urban and regional aerosols—I. model development, Atmos. Environ., 28(3), 531–546, doi:https://doi.org/10.1016/1352-2310(94)90129-5, 1994.

Wiedinmyer, C., Akagi, S. K., Yokelson, R. J., Emmons, L. K., Al-Saadi, J. A., Orlando, J. J. and Soja, A. J.: The Fire INventory from NCAR (FINN): A high resolution global model to estimate the emissions from open burning, Geosci. Model Dev., 4(3), 625–641, doi:10.5194/gmd-4-625-2011, 2011.

Xiu, A. and Pleim, J. E.: Development of a land surface model. Part I: Application in a mesoscale meteorological model, J. Appl. Meteorol., 40(2), 192–209, doi:10.1175/1520-0450(2001)040<0192:DOALSM>2.0.CO;2, 2001.

Yadav, P., Parde, A. N., Dhangar, N. G., Govardhan, G., Lal, D. M., Wagh, S., Prasad, D. S. V. V. D., Ahmed, R. and Ghude, S. D.: Understanding the genesis of a dense fog event over Delhi using observations and high-resolution model experiments, Model. Earth Syst. Environ., doi:10.1007/s40808-022-01463-x, 2022.

1167 Yadav, R., Bhatti, M. S., Kansal, S. K., Das, L., Gilhotra, V., Sugha, A., Hingmire, D., Yadav, S.,
1168 Tandon, A., Bhatti, R., Goel, A. and Mandal, T. K.: Comparison of ambient air pollution levels of
1169 Amritsar during foggy conditions with that of five major north Indian cities: multivariate analysis and
1170 air mass back trajectories, SN Appl. Sci., 2(11), 1–11, doi:10.1007/s42452-020-03569-2, 2020.

1171 Yu, H., Liu, S. C. and Dickinson, R. E.: Radiative effects of aerosols on the evolution of the
1172 atmospheric boundary layer, J. Geophys. Res. Atmos., 107(12), doi:10.1029/2001jd000754, 2002.

1173 Zaveri, R. A., Easter, R. C. and Peters, L. K.: A computationally efficient Multicomponent
1174 Equilibrium Solver for Aerosols (MESA), J. Geophys. Res. Atmos., 110(24), 1–22,
1175 doi:10.1029/2004JD005618, 2005.

1176 Zaveri, R. A., Easter, R. C., Fast, J. D. and Peters, L. K.: Model for Simulating Aerosol Interactions
1177 and Chemistry (MOSAIC), J. Geophys. Res. Atmos., 113(13), 1–29, doi:10.1029/2007JD008782,
1178 2008.

1179 Zhang, D. and Anthes, R. A.: A High-Resolution Model of the Planetary Boundary Layer—Sensitivity
1180 Tests and Comparisons with SESAME-79 Data, J. Appl. Meteorol. Climatol., 21(11), 1594–1609,
1181 doi:10.1175/1520-0450(1982)021<1594:AHRMOT>2.0.CO;2, 1982.

1182 Zhang, F., Li, Y., Li, Z., Sun, L., Li, R., Zhao, C., Wang, P., Sun, Y., Liu, X., Li, J., Li, P., Ren, G.
1183 and Fan, T.: Aerosol hygroscopicity and cloud condensation nuclei activity during the AC3Exp
1184 campaign: Implications for cloud condensation nuclei parameterization, Atmos. Chem. Phys., 14(24),
1185 13423–13437, doi:10.5194/acp-14-13423-2014, 2014a.

1186 Zhang, X., Musson-Genon, L., Dupont, E., Milliez, M. and Carissimo, B.: On the Influence of a
1187 Simple Microphysics Parametrization on Radiation Fog Modelling: A Case Study During ParisFog,
1188 Boundary-Layer Meteorol., 151(2), 293–315, doi:10.1007/s10546-013-9894-y, 2014b.

1189

1190

1191

1192

1193

1194

1195

1196

1197

1198

1199

1200

1201 Table 1 Experiment set-up for the study. Numbers in parentheses for the physics options denote the

1202 namelist settings of the WRF-Chem model.

1203

	EXP 1	EXP 2	EXP 3
Meteorology Initial /lateral boundary Condition:	*NCEP Final Analysis (GFS-FNL), 1° x1°, 6 hourly*	*ERA-Interim Project, 1.125° x 0.703°, 6 hourly*	*ERA-Interim Project, 1.125° x 0.703°, 6 hourly*
Physics Options			
Cloud Physics	*Morrison 2-mom (10)*	*Morrison 2- mom (10)*	*Morrison 2- mom (10)*
Longwave Radiation	*RRTMG scheme (4)*	*RRTMG scheme (4)*	*RRTMG scheme (4)*
Shortwave Radiation	*Goddard shortwave (2)*	*RRTMG scheme (4)*	*RRTMG scheme (4)*
Surface Layer Physics	*Revised MM5 Monin-Obukhov scheme (1)*	*Revised MM5 Monin-Obukhov scheme (1)*	*Pleim-Xiu (7)*
Surface Model	*unified Noah land-surface model (2)*	*NoahMP (4)*	*Pleim-Xiu (7)*
PBL Scheme	*YSU scheme (1)*	*YSU (1)*	*ACM2 (7)*
Convective Parameterization	*Grell-Freitas (3)*	*Grell-Freitas (3)*	*Grell-Freitas (3)*
	Continuous simulation	**Meteorology refreshed every 24 hr*	***Continuous simulation: Soil nudging included*

1204

1205

1206
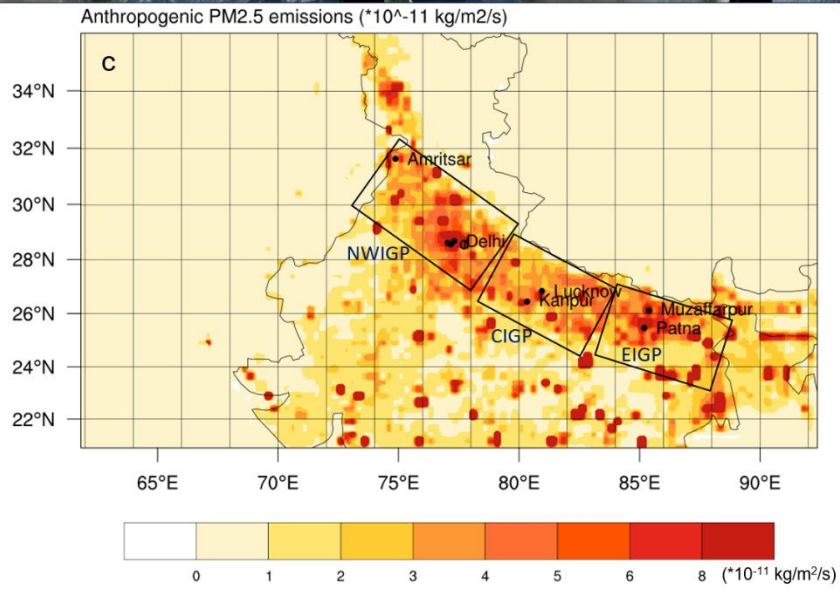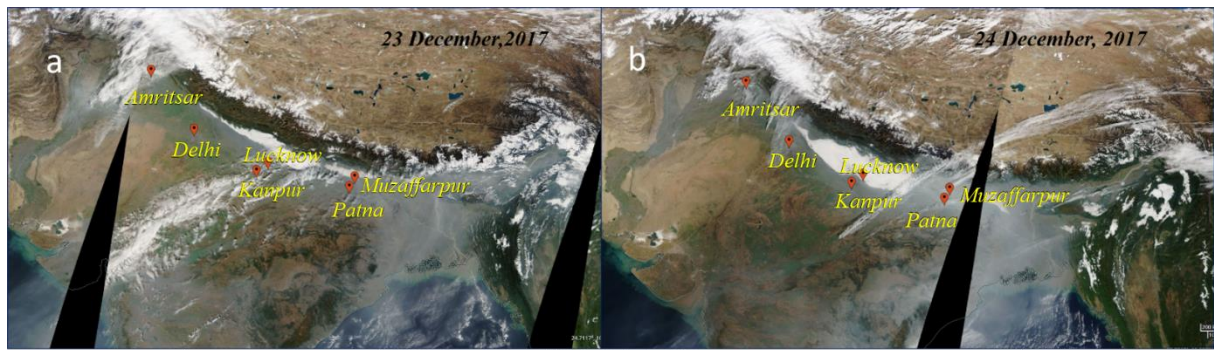
1207

Figure 1 The MODIS reflectance (true color) map representing low cloud over Indo Gangetic Plains, India (study region) indicative of likely fog and haze on 23rd December (a) and 24th December (b)2017. (c) Anthropogenic emission of PM$_{2.5}$ over IGP for December 2017 obtained from EDGAR-HTAP. The boxes represent the regions Northwest IGP (NWIGP), Central IGP (CIGP), and East IGP (EIGP).

1213

1214
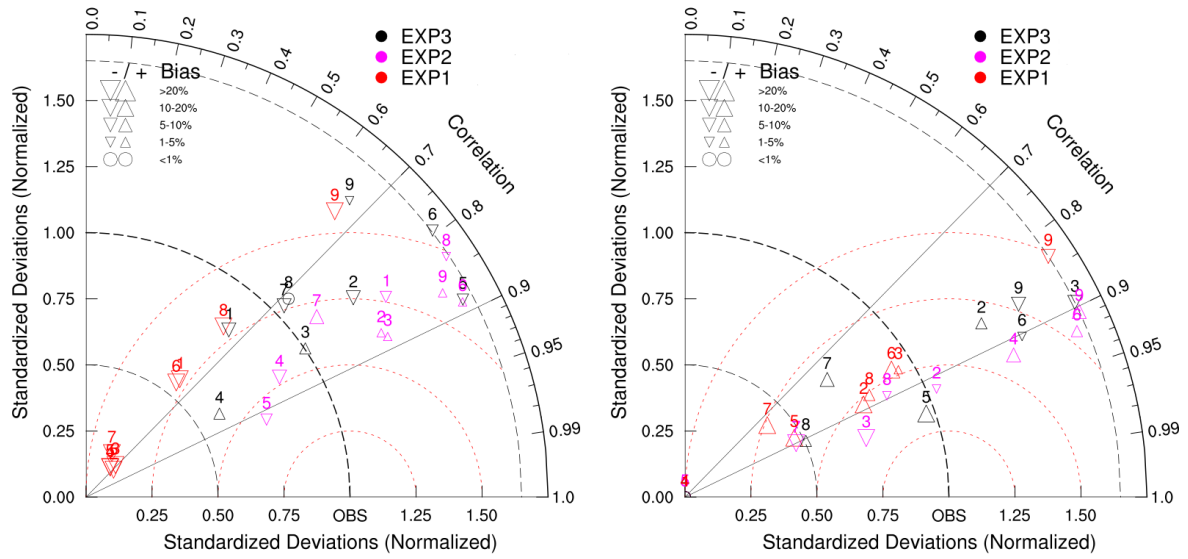
1215

1216

1217 Figure 2 Taylor Diagram of simulated (WRF-Chem) and observed (CPCB) relative humidity (left) and

1218 2-m temperature (right) over IGP. The colors indicate the experiments. The red dotted contours

1219 represent RMS values. The marker (triangles) size varies with a mean bias between the experiments

1220 and observation. Upside-down triangles represent positive bias (exp-obs) and vice versa. The stations

1221 over IGP are denoted by number 1. Amritsar, 2. IGI Airport (Delhi), 3. IHBAS (Delhi), 4. Dwarka

1222 (Delhi), 5. RKP (Delhi), 6. Kanpur, 7. Lucknow, 8. Patna, 9. Muzaffarpur. The locations are marked

1223 in Fig.1a.

1224
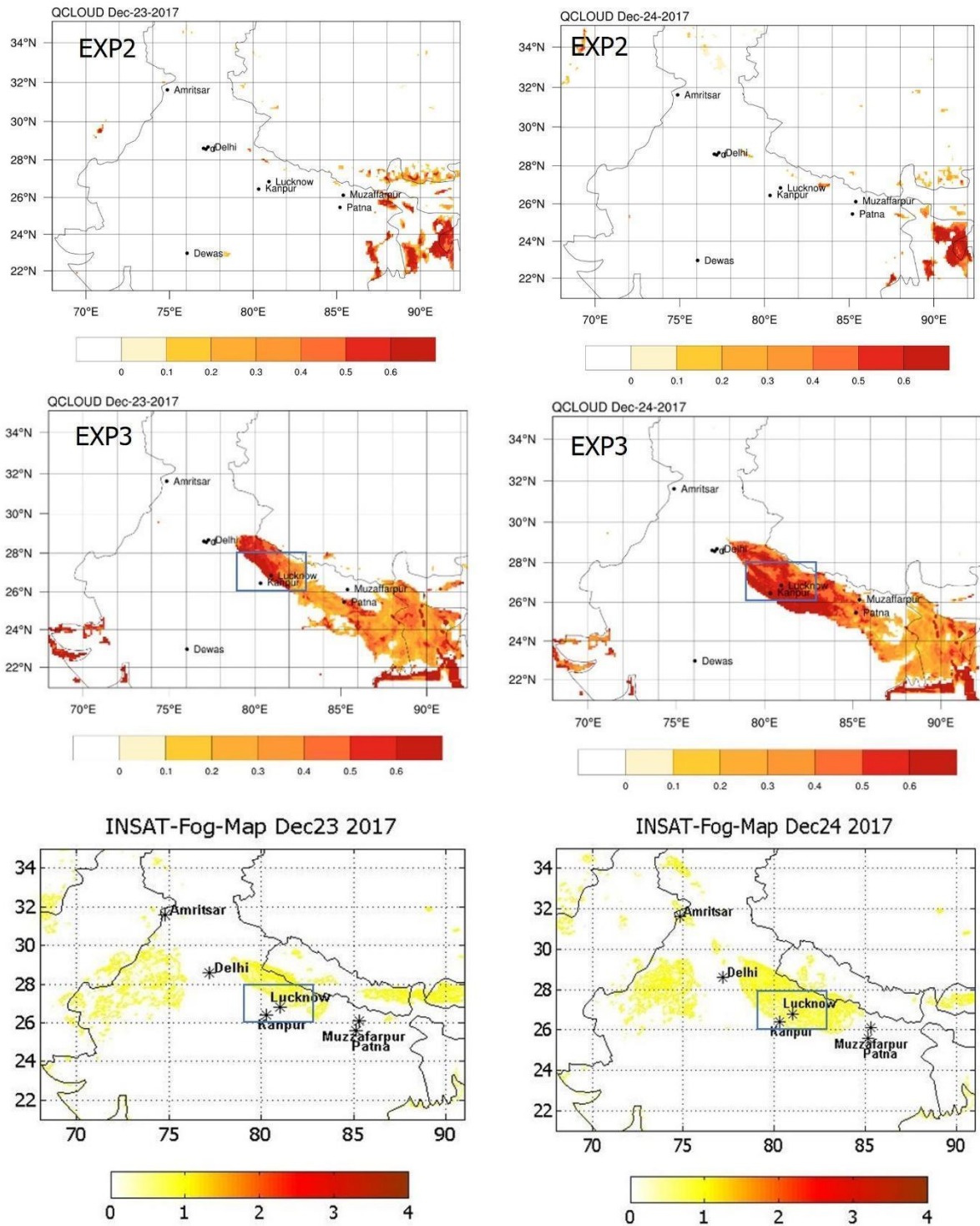
1225

Figure 3 Comparison of fog coverage from WRF-Chem and INSAT-3D satellite for 23 and 24 Dec

2017. WRF-Chem fog is represented by surface layer cloud water mixing ratios (in g m^{-3}) whereas

INSAT-3D provides fog intensity which varies from 0 to 4 indicating SHALLOW, MODERATE,

DENSE, and VERY_DENSE, respectively. The rectangle in central IGP is the region for the time

series analysis.

1231
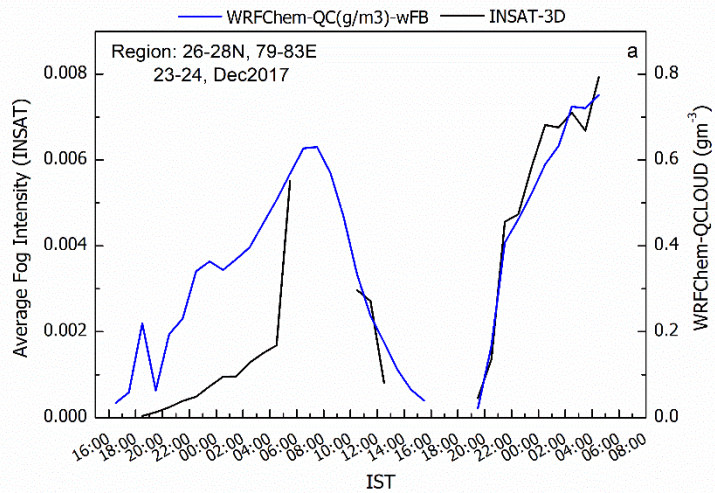
1232

1233 Figure 4 Average Hourly variation of fog on 23 and 24 December 2017 from WRF-Chem EXP3

1234 simulation and INSAT-3D satellite between 26°N-28°N,79°E-83°E (region shown in Fig 3). The time

1235 is in IST (Indian Standard Time; IST is 5.5 hours ahead of Universal Time Coordinate (UTC).

1236
1237
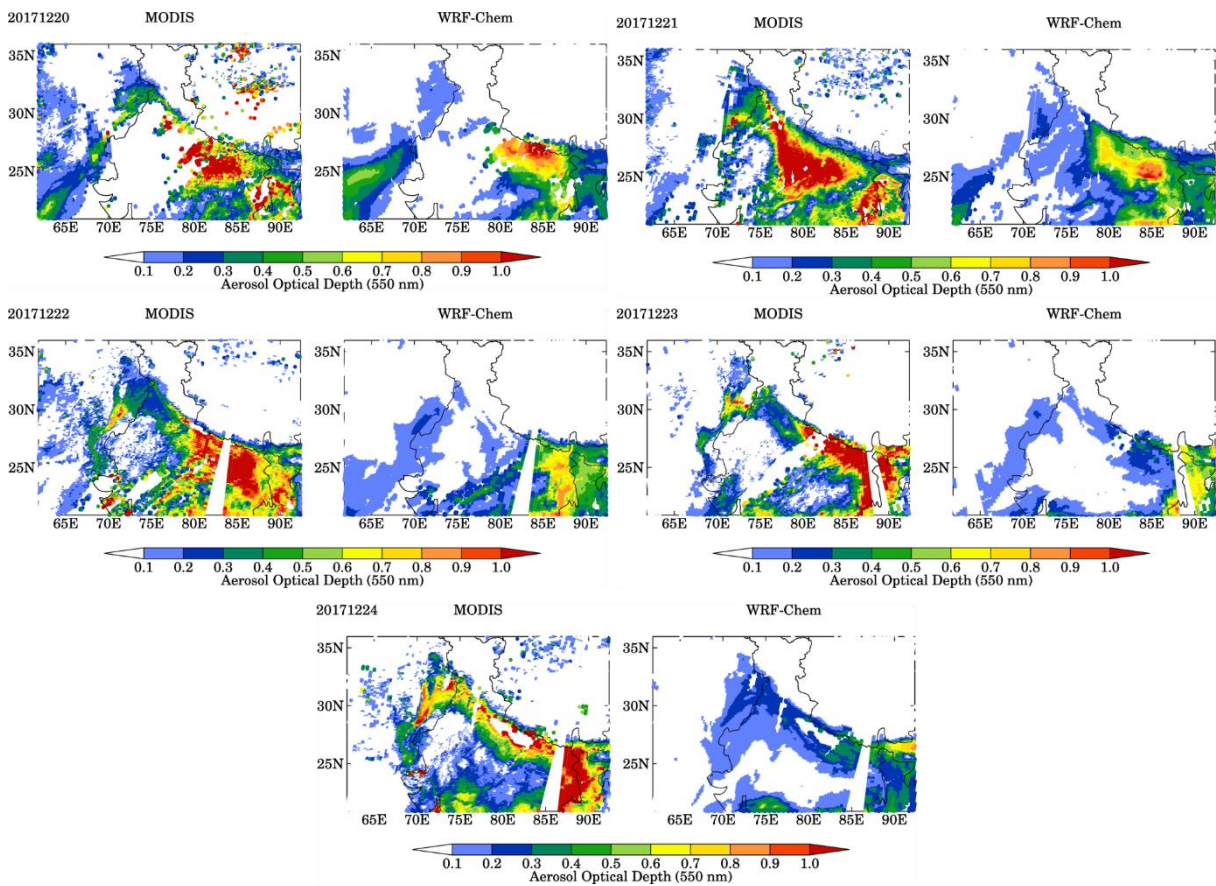
1238

1239 Figure 5 Comparison of WRF-Chem AOD with MODIS observation over the model domain on 20,
1240 21, 22, 23, and 24 December 2017.

1241

1242   .

1243
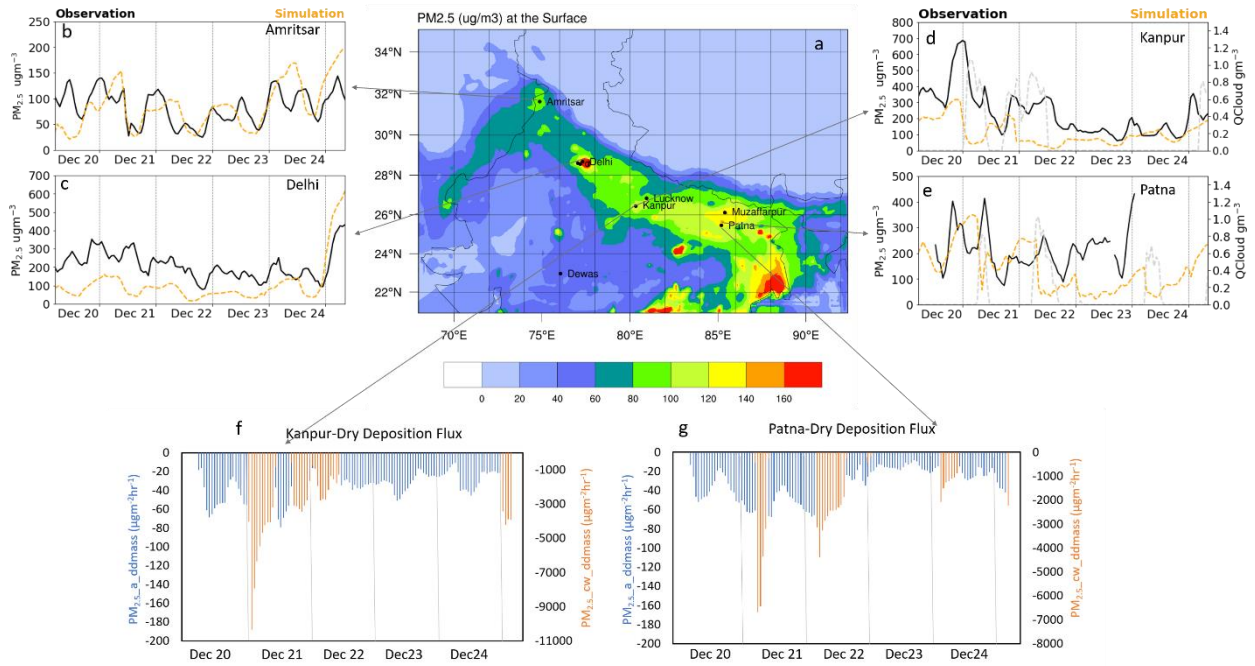
1244

1245   Figure 6 WRF-Chem simulated surface PM$_{2.5}$ map over IGP (a); comparison of WRF-Chem PM$_{2.5}$

1246   with CPCB observation for the period 20-24 Dec 2017 for (b) Amritsar, (c) Delhi, (d) Kanpur and (e)

1247   Patna. Dry Deposition rate of PM$_{2.5}$ for (f) Kanpur and (g) Patna. The grey dotted line in (d) Kanpur

1248   and (e) Patna is fog (QCloud) present during the study period.

1249
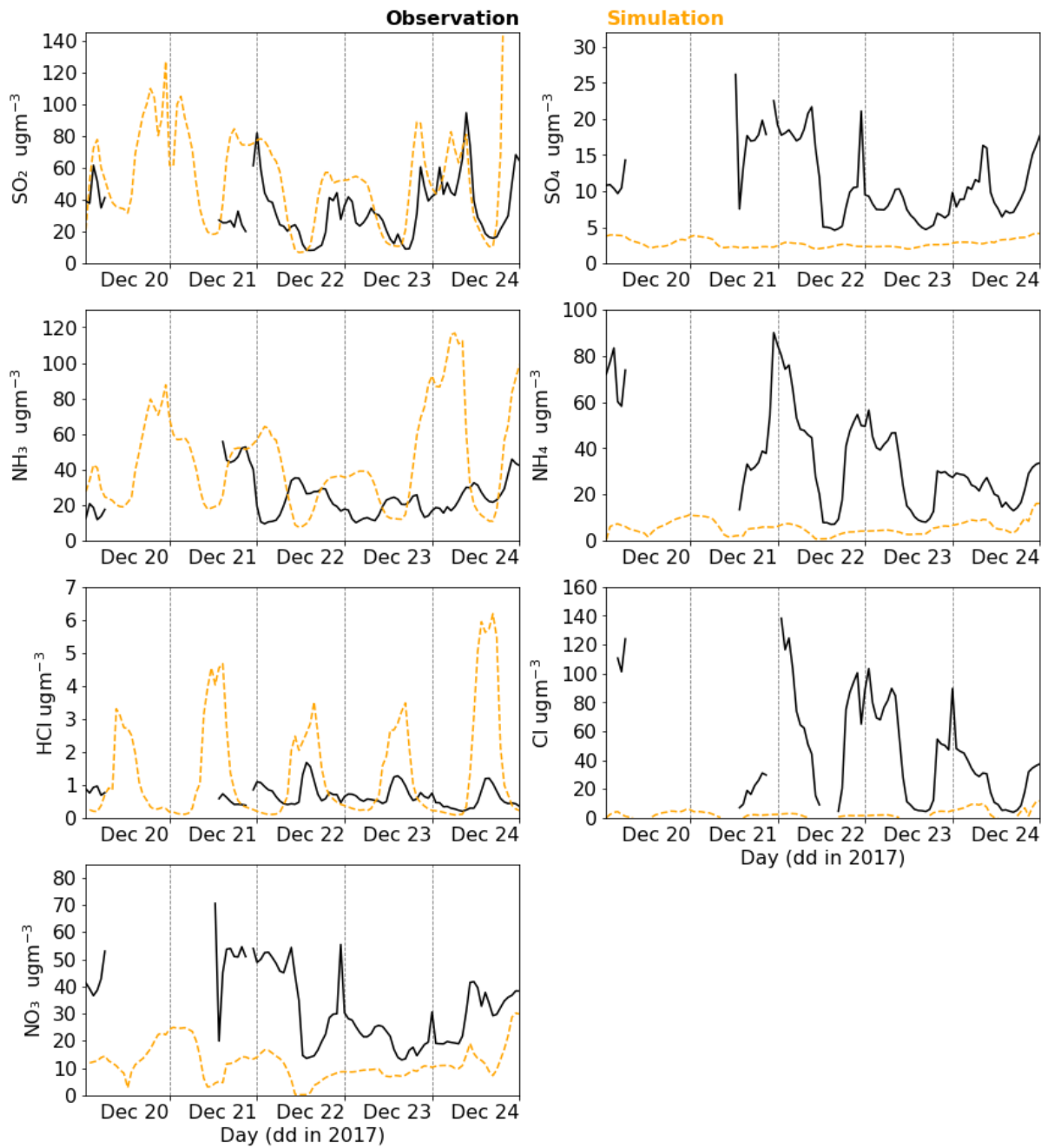
1250
1251   Figure 7 Comparison of WRF-Chem simulated ions (SO_4^{2-}, NH_4^+, NO_3^-, Cl^-) and trace gases (SO_2,

1252 NH_3 & HCl) with the observation from WIFEX campaign at Delhi.

1253

1254

1255
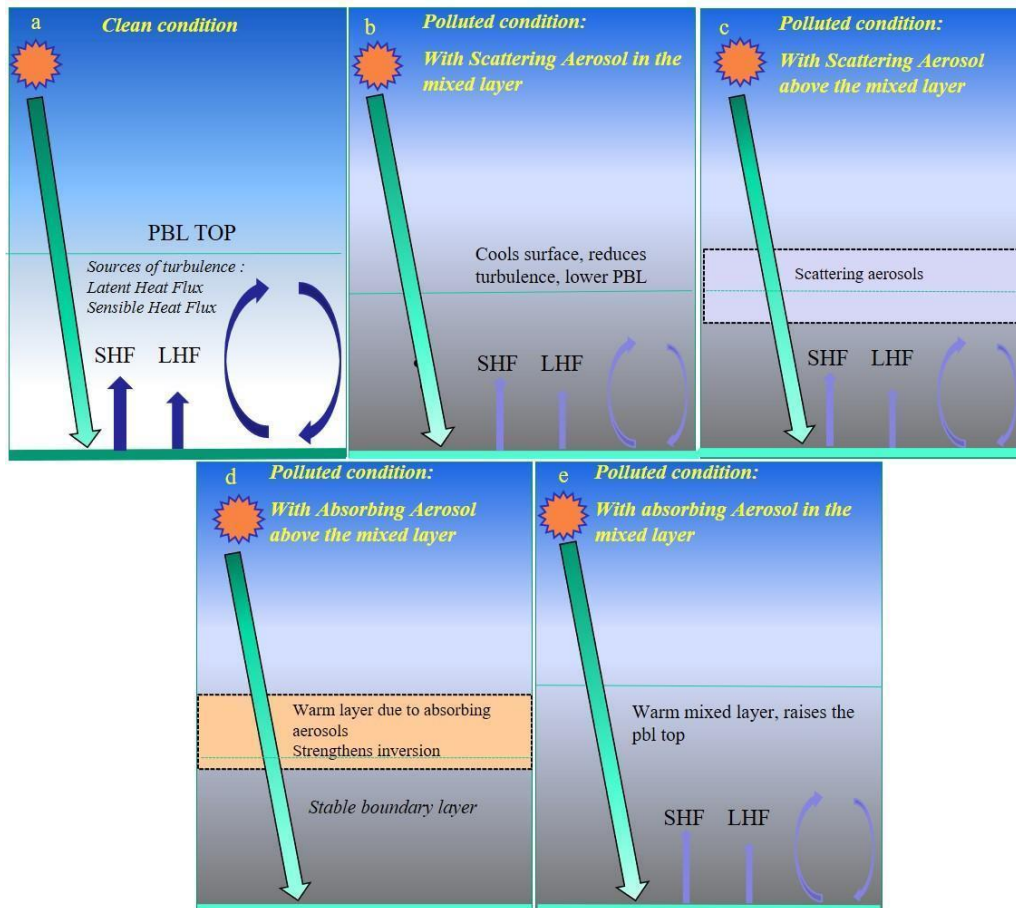
1256

1257   Figure 8 Schematic diagram of Aerosol Radiation Feedback.

1258

1259
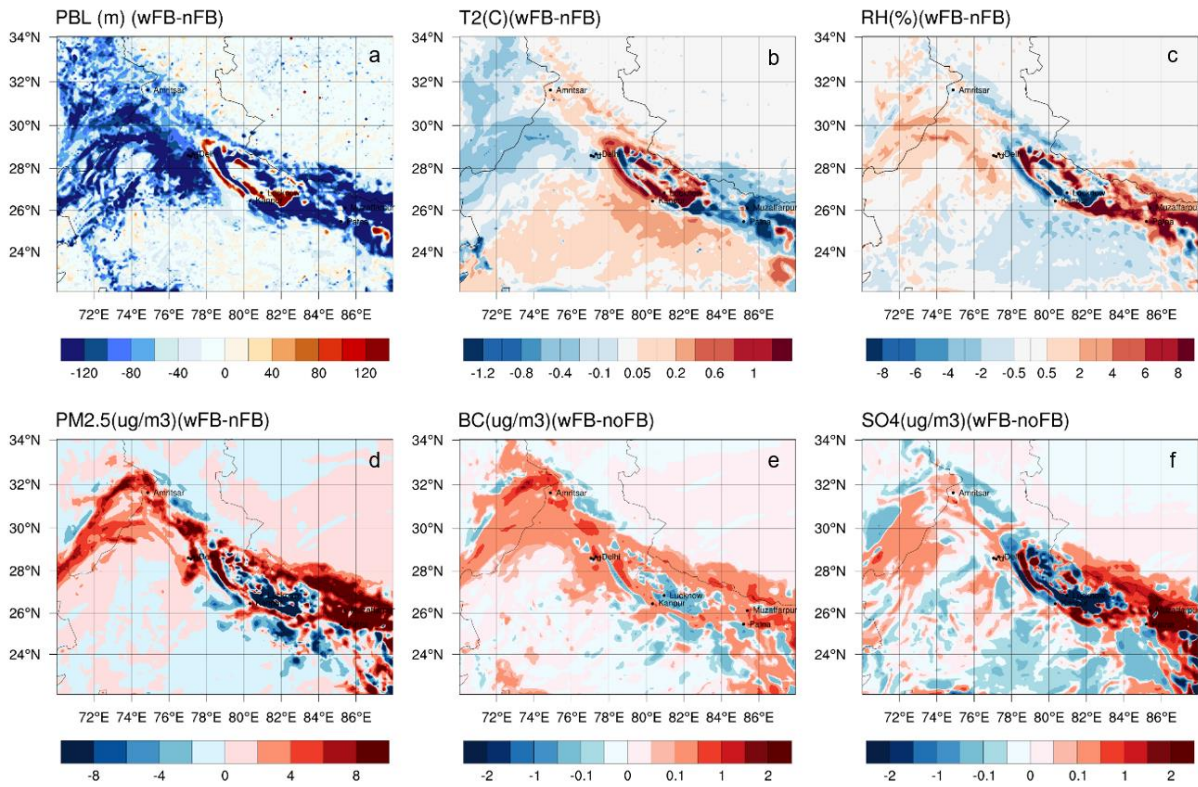
1260
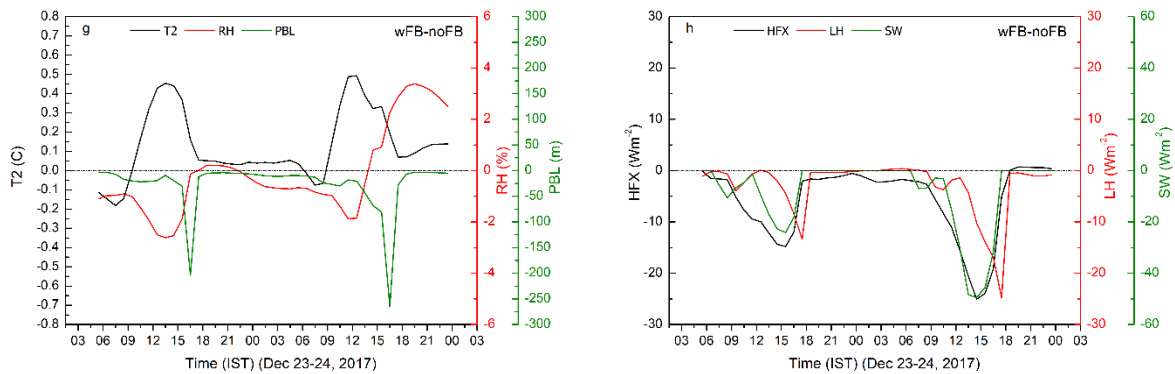
1261

Figure 9 Effect of Aerosol Radiation feedback (wFB-nFB) on (a) PBL height, (b) 2-m temperature, (c) 2-m relative humidity, (d) surface PM$_{2.5}$, (e) surface BC and (f) surface SO$_4$ for December 24 at local noon (13:30-15:30 IST). (g) The time series of ΔPBL, ΔT2, and ΔRH; (h) ΔHFX (sensible heat flux), ΔLH (latent heat flux), and ΔSWF (downward shortwave flux) over CIGP for December 23 and 24. Δ denotes the difference between with and without AR feedback (wFB-nFB).

1267
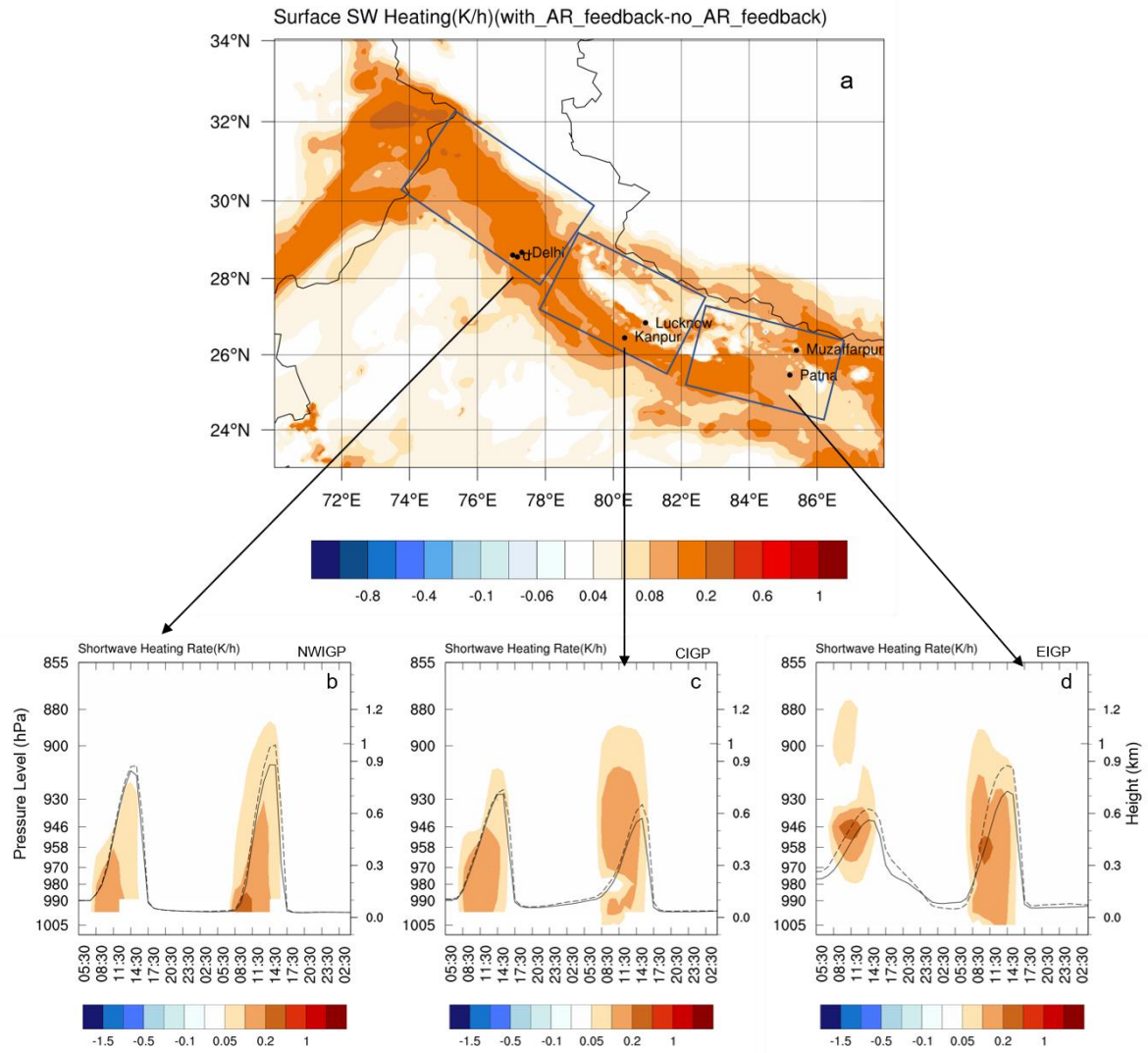
1268
1269

Figure 10 Differences in shortwave heating rates (K h⁻¹) between simulations with and without aerosol radiation feedback (a) at the surface, and for pressure-time cross-sections over (b) NWIGP, (c) CIGP. And (d) EIGP for December 23 and 24. The solid and dashed lines are the PBL height with and without AR feedback respectively. The time is in IST.
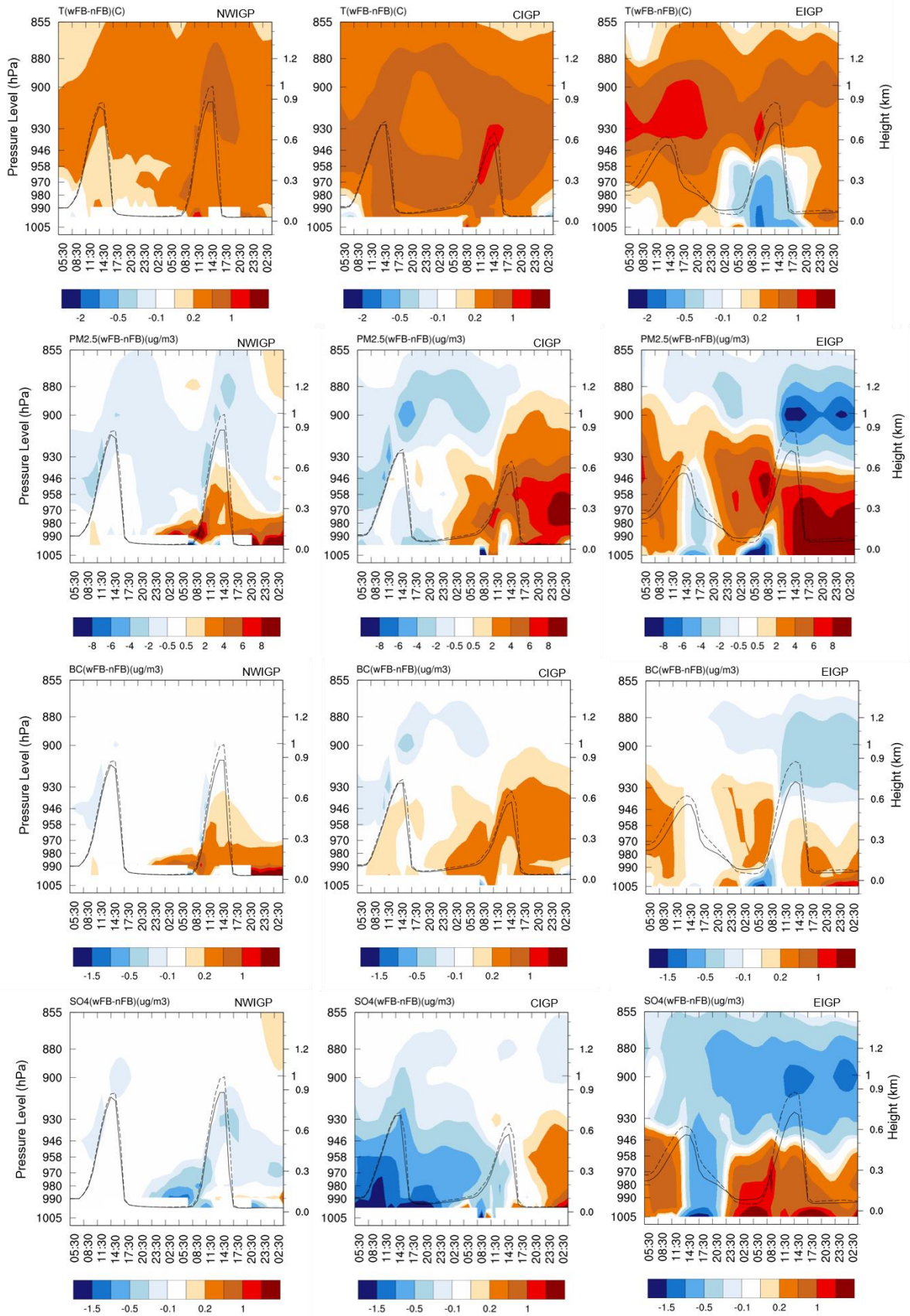
1274

1275

1276

1277   Figure 11 Pressure-time cross-section of the differences in T, $PM_{2.5}$, BC and SO_4^{2-} between

1278   simulations with and without the AR feedback for December 23 and 24. The solid and dashed lines

1279   are the PBL height with and without AR feedback respectively. The time is in IST.

1280

1281
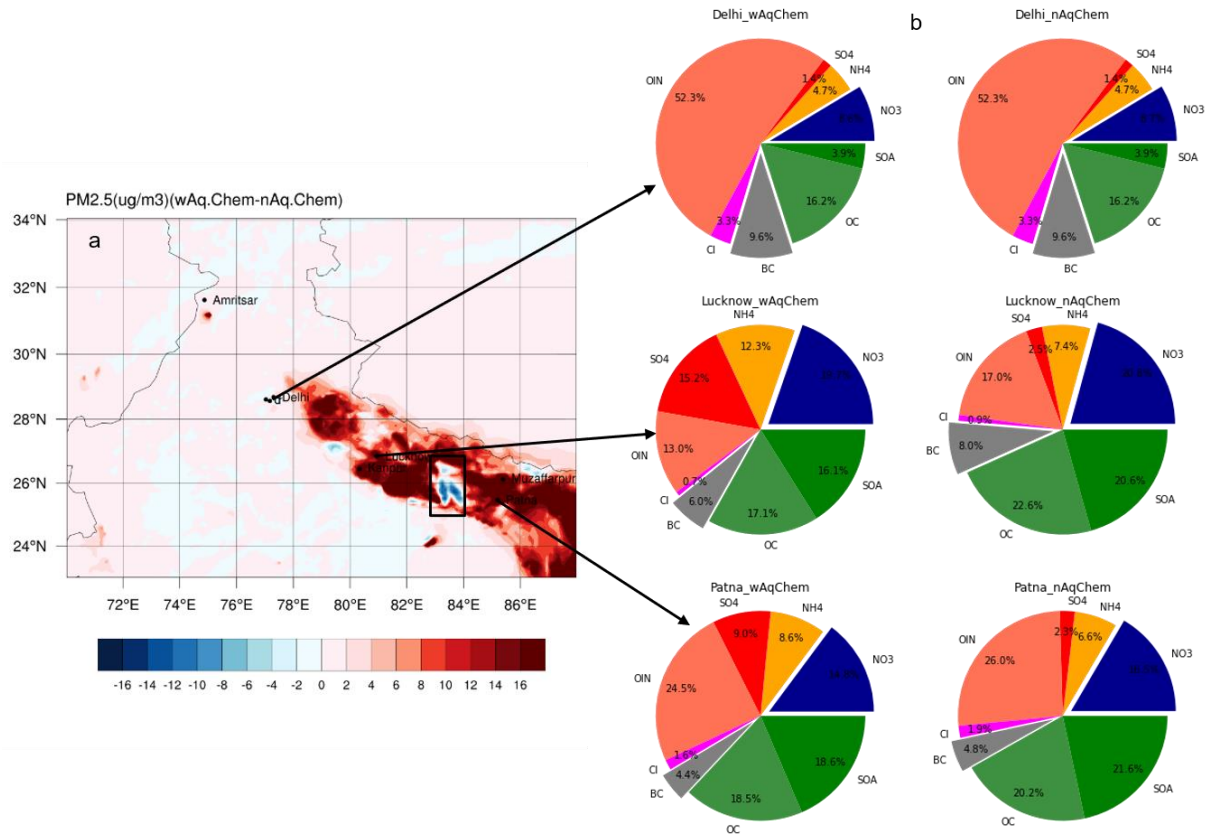
1282

1283   Figure 12 (a) Surface $\Delta PM_{2.5}$ (wAq.chem-noAq.chem) and (b) pie charts of $PM_{2.5}$ composition

1284   distribution for the two cases, with and without Aqueous phase Chemistry for 24 Dec 2017. The

1285   stations Delhi, Lucknow (LKN), and Patna are representative of NWIGP, CIGP, and EIGP regions

1286   respectively.

1287

1288

1289
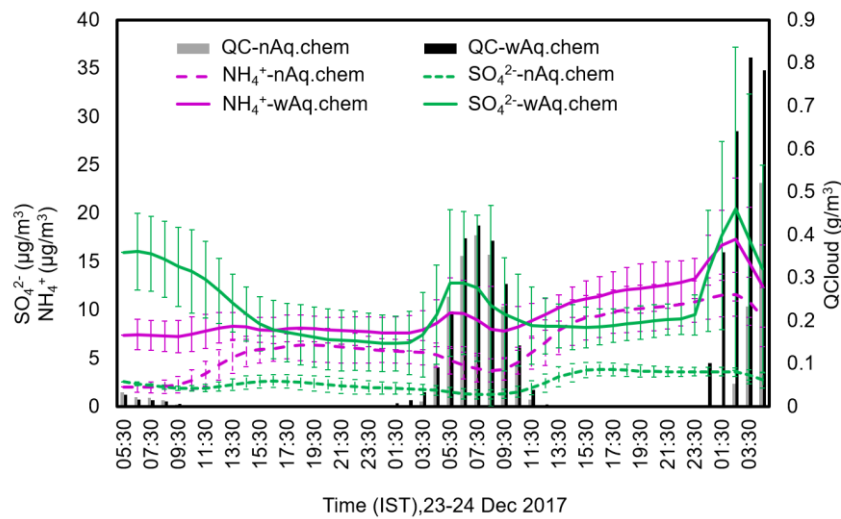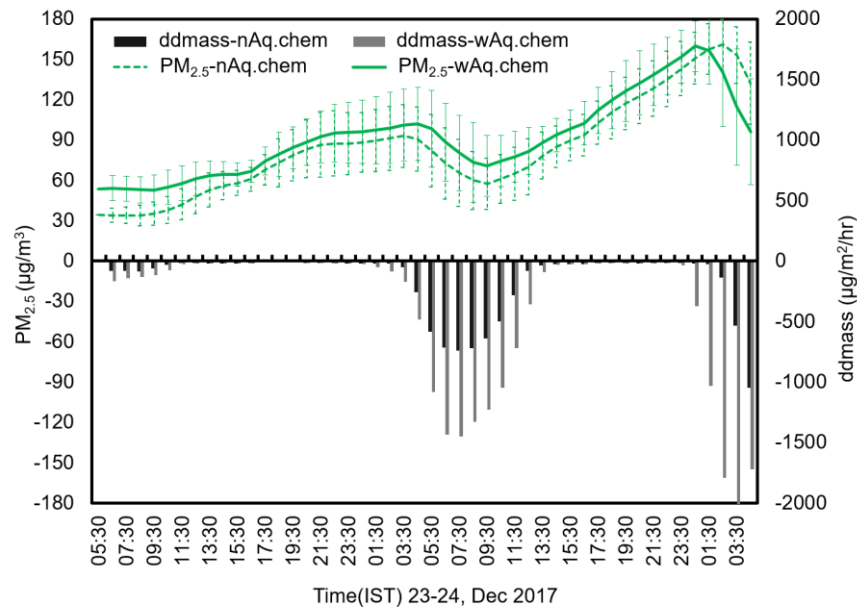
Figure 13 Time series of (a) PM$_{2.5}$ and its dry deposition (ddmass) flux change, (b) SO$_4^{2-}$, NH$_4^+$ and LWC (QCloud) with and without aqueous phase chemistry included in the model, averaged over the region bounded by a black rectangle in Fig. 12, for 23 and 24 December, 2017.

1296
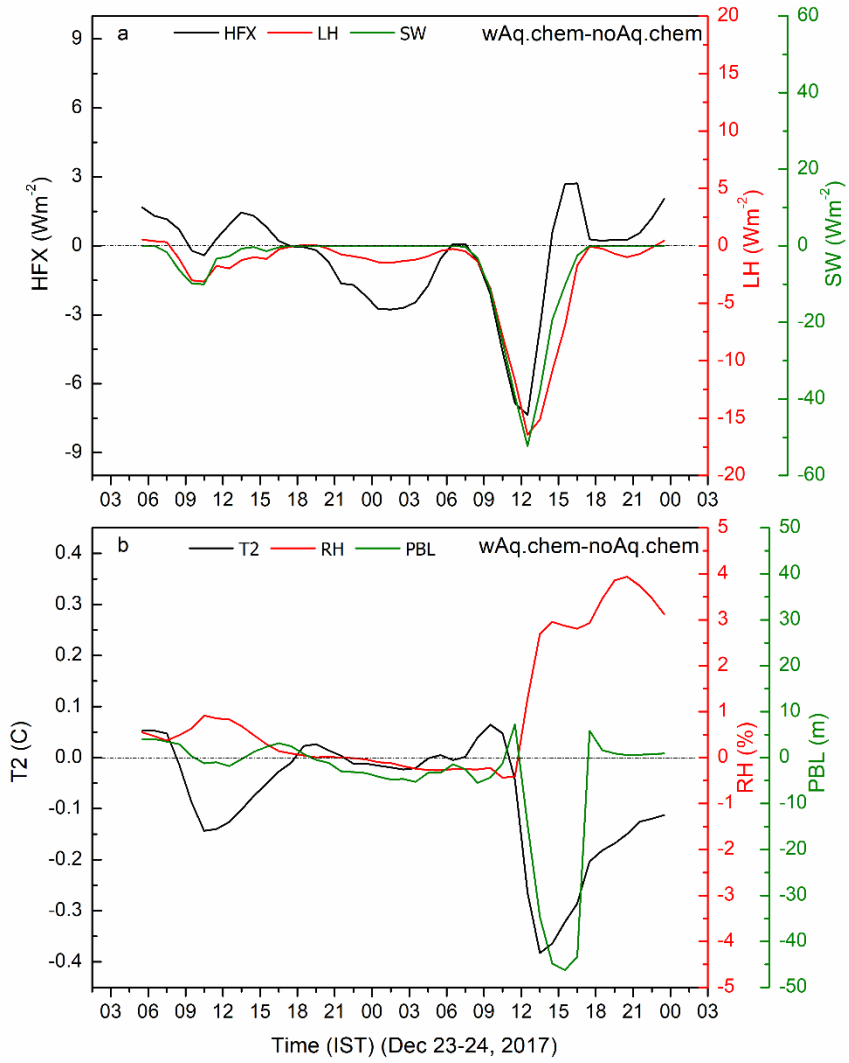
1297

Figure 14 Time series of (a) ΔHFX (sensible heat flux), ΔLH (latent heat flux), and ΔSWF
(downward shortwave flux); (b) ΔT2, ΔRH, and ΔPBL over CIGP (79E-83E,26N-28N), for
23 and 24 December, 2017. Δ denotes the difference between with and without aqueous phase
chemistry.

1302

1303
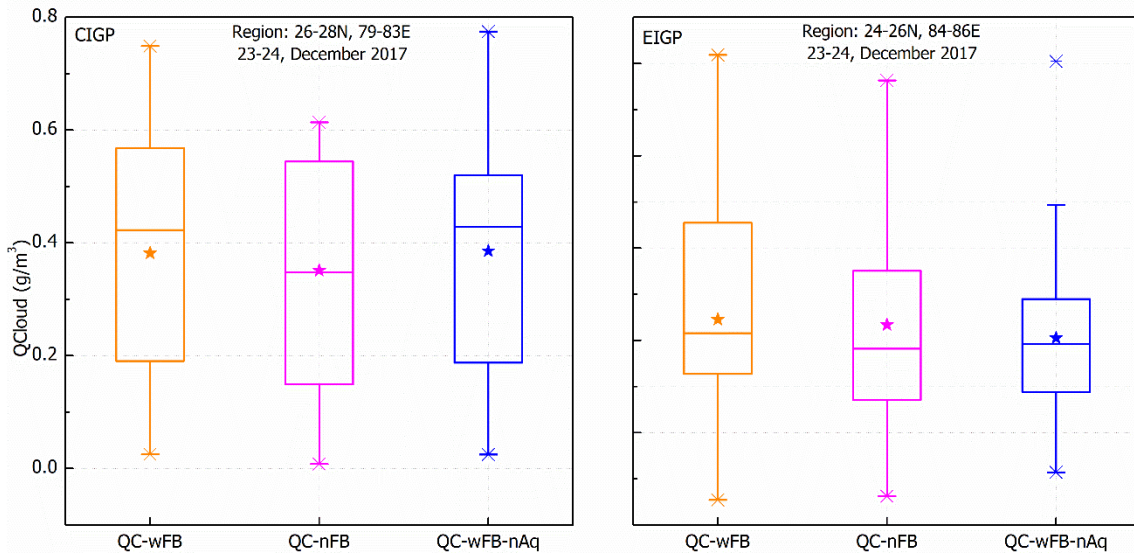
Figure 15 Averages (stars), medians (horizontal lines), quartiles (boxes), maxima, and minima for LWC (QCloud) averaged over CIGP (left panel) and EIGP (right panel) for the fog event on 23-24 December 2017. Gold is for the simulation with AR feedback and aqueous chemistry, magenta for the simulation with no AR feedback but includes aqueous chemistry, and blue for the simulation with AR feedback but no aqueous chemistry. WRF-Chem does not produce fog in the NWIGP during the study period.

Table 2: Table showing the start and end time of fog1 on 23-24 December 2017 with LWC for the sensitivity experiments, with AR feedback, no AR feedback and no Aqueous phase chemistry

Fog 1 (December 23-24, 2017)

	EXP-wFB			EXP-nFB			EXP-nAq.Chem		
	Start time	End time	Duration	Start time	End time	Duration	Start time	End time	Duration
	(IST)	(IST)	of Fog	(IST)	(IST)	of Fog	(IST)	(IST)	of Fog
CIGP	16:30	15:30	**23h**	18:30	17:30	**23h**	18:30	15:30	**21h**
LWC (g/m^3)	0.034	0.036±0.032		0.141±0.154	0.068±0.005		0.184±0.138	0.034 ±0.021	
Kanpur	05:30	13:30	**8h**	05:30	12:30	**7h**	05:30	12:30	**7h**
LWC (g/m^3)	0.334± 0.487	0.017		0.458±0.357	0.173± 0.071		0.533	0.025± 0.0123	
Lucknow	23:30	14:30	**15h**	00:30	14:30	**14h**	23:30	14:30	**15h**
LWC (g/m^3)	0.269±0.145	0.087±0.040		0.232±0.132	0.029±0.024		0.139±0.084	0.025±0.012	
EIGP	21:30	12:30	**15h**	23:30	10:30	**11h**	21:30	10:30	**13h**
LWC (g/m^3)	0.099±0.092	0.007		0.198±0.188	0.084±0.060		0.026±0.008	0.153±0.119	
Patna	00:30	12:30	**12h**	04:30	10:30	**6h**	02:30	10:30	**8h**
LWC (g/m^3)	0.100±0.090	0.007		0.009±0.005	0.038±0.041		0.196±0.198	0.166±0.130	
Muzzafarpur	05:30	11:30	**6h**	06:30	10:30	**4h**	06:30	09:30	**3h**
LWC (g/m^3)	0.112±0.146	0.043±0.057		0.051±0.041	0.003		0.142±0.151	0.157±0.064	

1329

1330 Table 2: Table showing the start time of fog 2 on 24 December 2017 with LWC for the sensitivity

1331 experiments, with AR feedback, no AR feedback and no Aqueous phase chemistry. Fog2 end time

1332 could not be noted as simulation ended on 25 December 2017, 00UT (5:30 IST) before fog2

1333 dissipates.

Fog 2 (December 24, 2017) Start time (IST)		
	EXP-wFB	**EXP-nFB**	**EXP-nAq.Chem**
CIGP	**19:30**	**20:30**	**21:30**
LWC (g/m^3)	0.025	0.008±0.007	0.025
Kanpur	21:30	22:30	23:30
LWC (g/m^3)	0.041±0.007	0.298±0.218	0.482±0.398
Lucknow	21:30	20:30	00:30
LWC (g/m^3)	0.203±0.165	0.005	0.229±0.209
EIGP	**00:30**	**01:30**	**01:30**
LWC (g/m^3)	0.024±0.030	0.072±0.088	0.014±0.009
Patna	03:30	03:30	03:30
LWC (g/m^3)	0.030± 0.046	0.018	0.060
Muzzafarpur	04:30	No fog	No fog
LWC (g/m^3)	0.159±0.038		

1334

1335

1336